Table 1
MiaPaCa-2 cell cDNAs isolated from 3T3 transformants

Clone ID #	Gene symbol	GenBank No.	Presence of entire ORF
1	CGI-152	NM_020410	Yes
2	RAB28	NM_004249	Yes
3	MRPL43	NM_032112	Yes
4	LTBR	NM_002342	No
5	UBQLN1	NM_013438	Yes
6	TBC1D2	NM_018421	Yes
7	FKBP10	NM_021939	Yes
8	HCCA2	NM_053005	Yes
9	Unknown	AK123415	ND
10	KRAS2	NM_004985	Yes
11	STK11IP	NM_052902	Yes
12	Unknown	AA627562	ND
13	PFKP	NM_002627	Yes

ORF, open reading frame; ND, not determined.

extensively investigated [3], little is known of such activity for *LTBR*. We thus focused on *LTBR* for further analysis.

Identification of a truncated form of LTBR

Although the nucleotide sequence of both ends of our LTBR cDNA was identical to that of human *LTBR*, the size of our cDNA (1452 bp) was smaller than that (2136 bp) of the full-length cDNA previously described. We thus determined the complete nucleotide sequence of our cDNA, revealing that it starts at nucleotide position 685 of the reported sequence (NM_002342). The longest open reading frame in our cDNA begins at amino acid position 221 and ends at position 435 of the previously described LTBR protein; it therefore encodes a predicted protein of 215 amino acids with a calculated molecular mass of 22,692 Da (Fig. 2). Given that the nucleotide sequence surrounding the putative translation start site of our cDNA matches the consensus Kozak motif, the corresponding mRNA likely produces this NH_2-terminally truncated form of LTBR, which is hereafter referred to as short-type LTBR.

5′-RACE analysis of LTBR mRNA

To confirm the presence of an mRNA encoding short-type LTBR in MiaPaCa-2 cells, we performed 5′-RACE to determine the 5′ ends of LTBR mRNAs. The first strand of LTBR cDNAs was generated with an LTBR-specific reverse transcription (RT) primer (Fig. 2) from RNA isolated from MiaPaCa-2 cells. Poly(A) was added to the 3′ end of the cDNAs, which were then subjected to nested PCR in order to amplify the 5′ ends. PCR products (ranging from a few hundred to 2000 bp) were detected only when reverse transcriptase was included in the procedure (Fig. 3A), indicating that the products were synthesized from cDNA, not from genomic DNA. The nucleotide sequence of 96 randomly chosen PCR products was determined. Sixty-eight of the 96 products matched the LTBR cDNA sequence and the positions of their 5′ ends are indicated in Fig. 3B. Transcription of most of the mRNAs corresponding to these PCR products was initiated in the region immediately upstream of the translation start site for short-type LTBR, indicating the existence of multiple mRNAs for this truncated protein in vivo.

Confirmation of transforming activity of short-type LTBR

To confirm the transforming activity of short-type LTBR, we examined its effect on anchorage-independent growth of 3T3 cells in soft agar. Whereas cells infected with an empty virus did not grow in soft agar, those infected with a virus encoding short-type LTBR formed multiple foci in repeated experiments (Fig. 4A). In addition, 3T3 cells expressing activated *KRAS2* readily grew in the agar.

We also injected the infected cells into nude mice. Tumors formed at all ($n = 10$) sites injected with 3T3 cells expressing short-type LTBR (Fig. 4B). Again, 3T3 cells expressing activated *KRAS2* also generated tumors at a high frequency, whereas those infected with the empty virus did not induce tumor formation. Together, these results thus confirmed that short-type LTBR possesses transforming activity.

Transforming activity of wild-type LTBR

To determine whether the full-length (435-amino acid) LTBR protein also possesses oncogenic potential, we performed the focus formation assay and in vivo tumorigenicity assay with a recombinant retrovirus encoding the wild-type

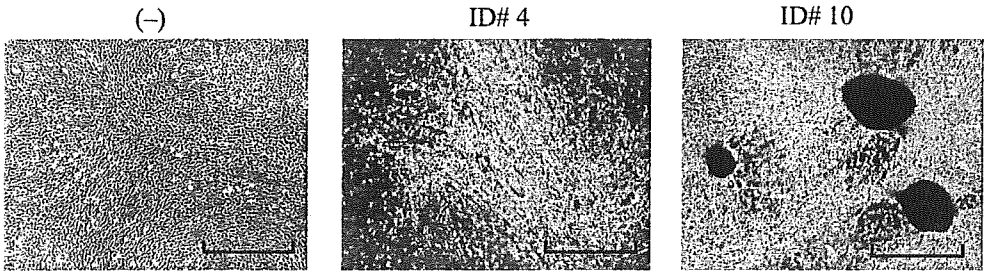

Fig. 1. Identification of transforming genes of MiaPaCa-2 cells. Mouse 3T3 cells were infected with an empty retrovirus (–) or with recombinant retroviruses harboring cDNAs corresponding to library clones ID #4 (short-type LTBR) or ID #10 (KRAS2). The cells were photographed after culture for 2 weeks. Scale bars, 1 mm.

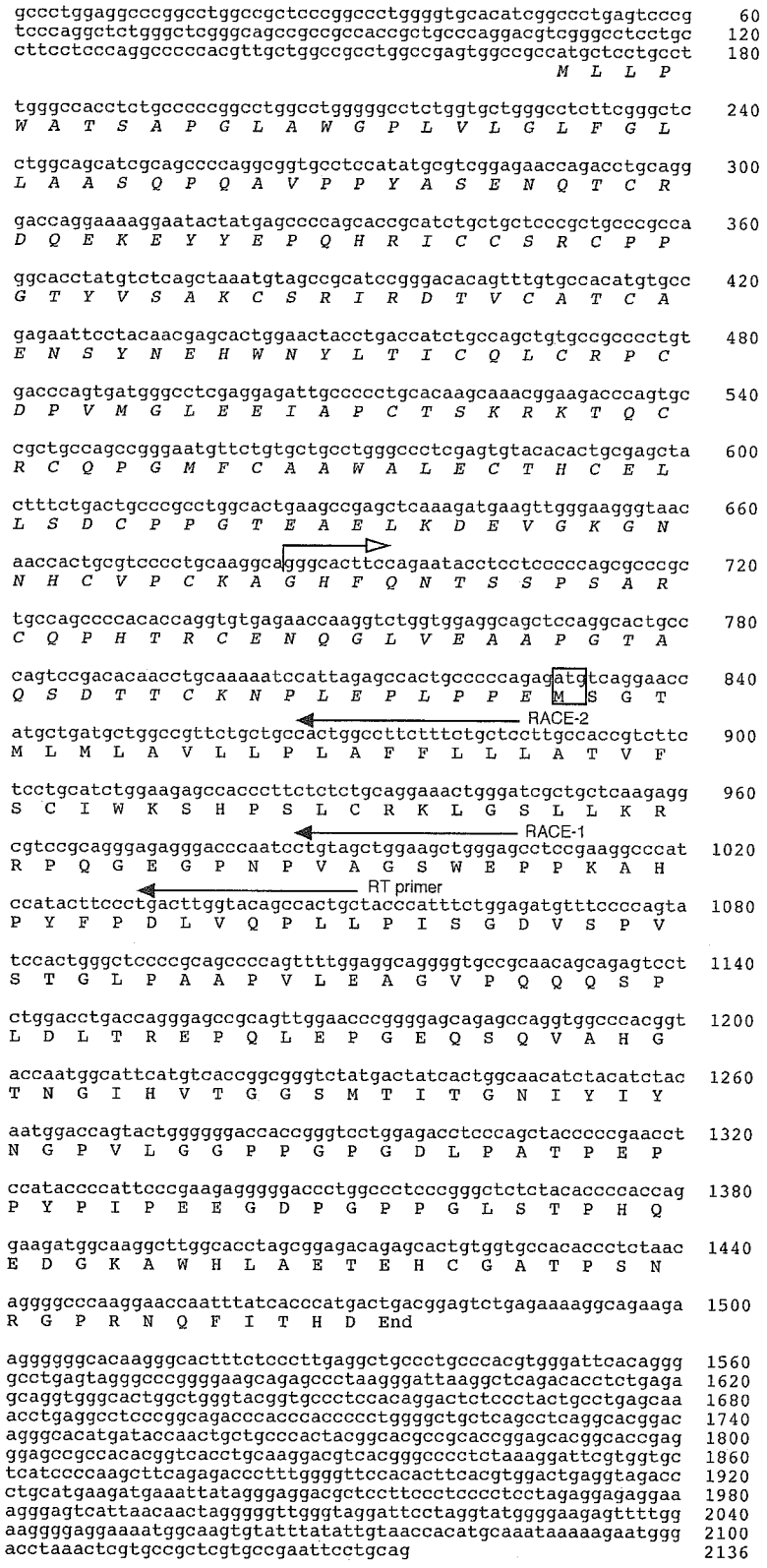

Fig. 2. Characterization of an LTBR cDNA isolated by screening for transformation activity. Amino acid residues of the full-length LTBR protein are aligned with the previously determined nucleotide sequence of LTBR cDNA (NM_002342). The cDNA isolated in the present study begins at nucleotide position 685 (open arrow) of the reported cDNA. The putative translation start site for the truncated (short-type) LTBR protein is boxed. The positions of primers used for 5′-RACE are indicated by closed arrows.

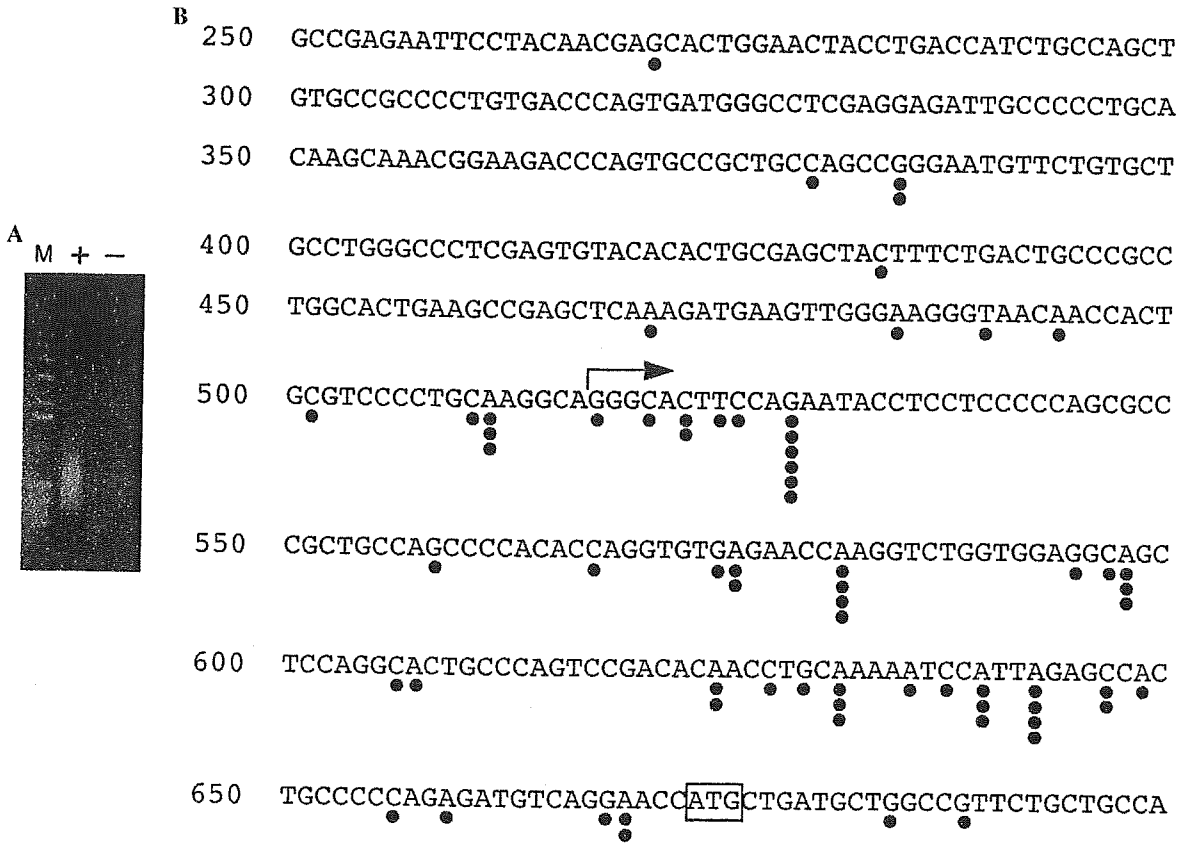

Fig. 3. 5′-RACE analysis of LTBR cDNA. (A) Total RNA of MiaPaCa-2 cells was incubated with the LTBR-specific RT primer in the presence (+) or absence (−) of reverse transcriptase, and resulting cDNA was subjected to PCR-based 5′-RACE. The PCR products were fractionated by electrophoresis through a 1.8% agarose gel and stained with ethidium bromide. Lane M, 1-kb DNA ladder. (**B**) The positions of the 5′ ends of 5′-RACE products are indicated by closed circles in alignment with the reported LTBR cDNA sequence. Numbers on the left indicate nucleotide positions relative to the translation initiation site of the full-length (wild-type) cDNA. The arrow indicates the 5′ end of the cDNA isolated by retroviral screening in the present study; the putative translation start codon of this cDNA is boxed.

human protein. The infected cells generated both transformed foci in vitro and tumors in nude mice (Fig. 5).

Discussion

In the present study, we constructed a retroviral cDNA expression library for a PDC cell line. Given that 80% (24/30) of the viral plasmids contained cDNA inserts and that the overall clone number was >1 million, this library should represent most of the mRNAs in MiaPaCa-2 cells. We infected 3T3 mouse fibroblasts with this recombinant library to screen for transforming genes with a focus formation assay. This screen identified *KRAS2* with an activating mutation as a transforming gene of MiaPaCa-2 cells, supporting the fidelity of our approach.

Our screen also identified a transforming cDNA that encodes an NH_2-terminally truncated form of LTBR. 5′-RACE analysis revealed the existence of mRNAs for this short-type LTBR in MiaPaCa-2 cells, and retrovirus-mediated expression of the isolated cDNA in 3T3 cells conferred the ability to grow in soft agar in vitro as well as the ability to form tumors in vivo.

LTBR belongs to the tumor necrosis factor (TNF) receptor superfamily [9] and binds two functional ligands, lymphotoxin-α1β2 and LIGHT [10,11]. LTBR is expressed by many cell types (but not by lymphocytes), whereas expression of the LTBR ligands is restricted to activated lymphocytes [11]. Signaling by LTBR is important in the development of lymphoid tissue and in generation of adaptive humoral immune responses [12,13]. In general, LTBR function is thought to be linked to apoptosis. Indeed, activation of LTBR by its endogenous ligands or by anti-receptor antibodies triggers the death of various tumor cell lines [14,15]. Activation of the LIGHT-LTBR signaling pathway in tumor cells also induces marked chemokine-dependent recruitment of T cells to tumors, resulting in the rejection of established tumor cells [16].

LTBR activation has also been linked to tumor development, however. Its activation in fibrosarcoma cells thus induces angiogenesis and tumor growth by triggering the release of macrophage inflammatory protein-2, an angiogenic CXC chemokine [17]. Although oncogenic potential has not previously been demonstrated for LTBR, our data now show that both the full-length and truncated forms of this protein possess transforming activity even in the absence of exogenous cognate ligands. A high level of expression of LTBR conferred by the retroviral long terminal repeat in our experiments might have resulted in self-oligomerization

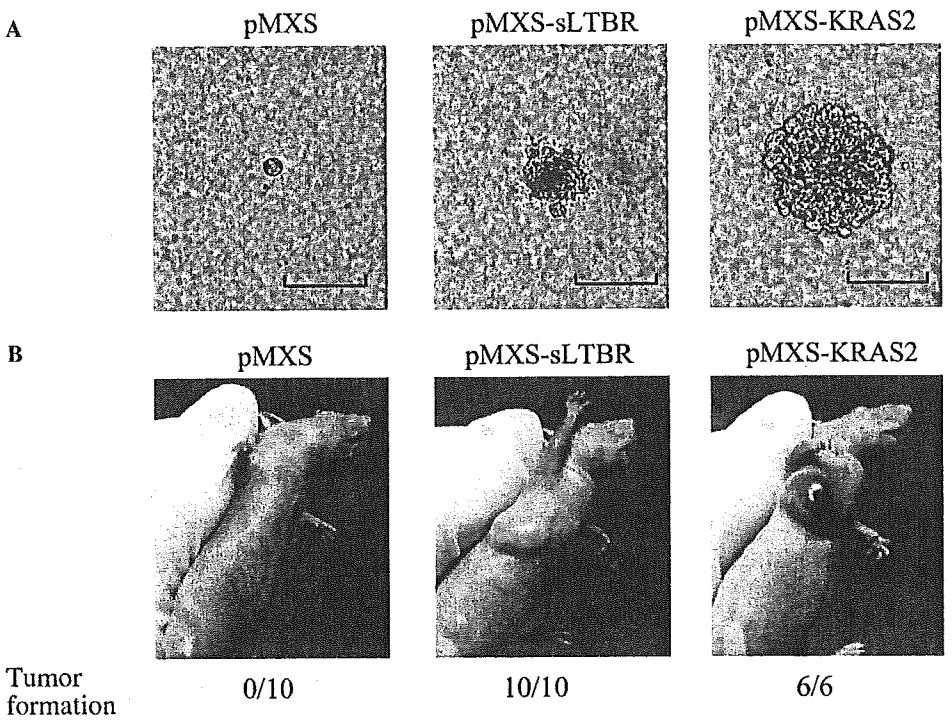

Fig. 4. Transforming activity of short-type LTBR. (A) Focus formation assay. 3T3 cells infected either with empty retrovirus (pMXS) or with retroviruses encoding short-type LTBR (pMXS-sLTBR) or activated KRAS2 (pMXS-KRAS2) were seeded into soft agar and incubated for 2 weeks. Scale bars, 100 μm. (B) Tumorigenicity assay. Cells infected as in (A) were injected into the shoulder of nude mice and tumor formation was examined after 3 weeks. The frequency of tumor formation determined is indicated.

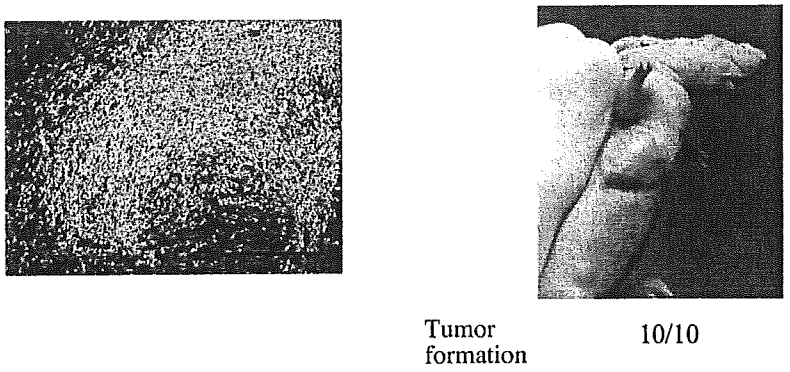

Fig. 5. Transforming activity of full-length LTBR. The transforming activity of a retroviral vector encoding full-length (wild-type) LTBR was evaluated by the focus formation assay (left) or the in vivo tumorigenicity assay (right). Scale bar, 1 mm.

of the protein. It is thus likely that LTBR exerts its oncogenic function in a tissue- and context-dependent manner. As shown here for PDC, it will be important to determine whether LTBR also contributes to the mechanism of transformation in other human malignancies.

Acknowledgments

This work was supported in part by a grant for Third-Term Comprehensive Control Research for Cancer from the Ministry of Health, Labor, and Welfare of Japan as well as by a grant for "High-Tech Research Center" Project for Private Universities: Matching Fund Subsidy (2002–2006) from the Ministry of Education, Culture, Sports, Science and Technology of Japan.

References

[1] S. Rosewicz, B. Wiedenmann, Pancreatic carcinoma, Lancet 349 (1997) 485–489.
[2] P.C. Bornman, I.J. Beckingham, Pancreatic tumours, Br. Med. J. 322 (2001) 721–723.
[3] M. Tada, M. Omata, M. Ohto, Clinical application of ras gene mutation for diagnosis of pancreatic adenocarcinoma, Gastroenterology 100 (1991) 233–238.
[4] S.R. Bramhall, The use of molecular technology in the differentiation of pancreatic cancer and chronic pancreatitis, Int. J. Pancreatol. 23 (1998) 83–100.

[5] G. Schneider, J.T. Siveke, F. Eckel, R.M. Schmid, Pancreatic cancer: basic and clinical aspects, Gastroenterology 128 (2005) 1606–1625.
[6] A. Yanagisawa, K. Ohtake, K. Ohashi, M. Hori, T. Kitagawa, H. Sugano, Y. Kato, Frequent c-Ki-ras oncogene activation in mucous cell hyperplasias of pancreas suffering from chronic inflammation, Cancer Res. 53 (1993) 953–956.
[7] S.A. Aaronson, Growth factors and cancer, Science 254 (1991) 1146–1153.
[8] M.A. Frohman, M.K. Dush, G.R. Martin, Rapid production of full-length cDNAs from rare transcripts: amplification using a single gene-specific oligonucleotide primer, Proc. Natl. Acad. Sci. USA 85 (1988) 8998–9002.
[9] P.D. Crowe, T.L. VanArsdale, B.N. Walter, C.F. Ware, C. Hession, B. Ehrenfels, J.L. Browning, W.S. Din, R.G. Goodwin, C.A. Smith, A lymphotoxin-β-specific receptor, Science 264 (1994) 707–710.
[10] J.L. Browning, I.D. Sizing, P. Lawton, P.R. Bourdon, P.D. Rennert, G.R. Majeau, C.M. Ambrose, C. Hession, K. Miatkowski, D.A. Griffiths, A. Ngam-ek, W. Meier, C.D. Benjamin, P.S. Hochman, Characterization of lymphotoxin-αβ complexes on the surface of mouse lymphocytes, J. Immunol. 159 (1997) 3288–3298.
[11] W.R. Force, B.N. Walter, C. Hession, R. Tizard, C.A. Kozak, J.L. Browning, C.F. Ware, Mouse lymphotoxin-β receptor. Molecular genetics, ligand binding, and expression, J. Immunol. 155 (1995) 5280–5288.
[12] A. Futterer, K. Mink, A. Luz, M.H. Kosco-Vilbois, K. Pfeffer, The lymphotoxin β receptor controls organogenesis and affinity maturation in peripheral lymphoid tissues, Immunity 9 (1998) 59–70.
[13] R.M. Locksley, N. Killeen, M.J. Lenardo, The TNF and TNF receptor superfamilies: integrating mammalian biology, Cell 104 (2001) 487–501.
[14] J.L. Browning, K. Miatkowski, I. Sizing, D. Griffiths, M. Zafari, C.D. Benjamin, W. Meier, F. Mackay, Signaling through the lymphotoxin β receptor induces the death of some adenocarcinoma tumor lines, J. Exp. Med. 183 (1996) 867–878.
[15] I.A. Rooney, K.D. Butrovich, A.A. Glass, S. Borboroglu, C.A. Benedict, J.C. Whitbeck, G.H. Cohen, R.J. Eisenberg, C.F. Ware, The lymphotoxin-β receptor is necessary and sufficient for LIGHT-mediated apoptosis of tumor cells, J. Biol. Chem. 275 (2000) 14307–14315.
[16] P. Yu, Y. Lee, W. Liu, R.K. Chin, J. Wang, Y. Wang, A. Schietinger, M. Philip, H. Schreiber, Y.X. Fu, Priming of naive T cells inside tumors leads to eradication of established tumors, Nat. Immunol. 5 (2004) 141–149.
[17] T. Hehlgans, B. Stoelcker, P. Stopfer, P. Muller, G. Cernaianu, M. Guba, M. Steinbauer, S.A. Nedospasov, K. Pfeffer, D.N. Mannel, Lymphotoxin-β receptor immune interaction promotes tumor growth by inducing angiogenesis, Cancer Res. 62 (2002) 4034–4040.

Frag1, a homolog of alternative replication factor C subunits, links replication stress surveillance with apoptosis

Hideshi Ishii*, Taeko Inageta*, Koshi Mimori†, Toshiyuki Saito‡, Hiroki Sasaki§, Masaharu Isobe¶, Masaki Mori†, Carlo M. Croce‖**, Kay Huebner‖, Keiya Ozawa*, and Yusuke Furukawa*

*Center for Molecular Medicine, Jichi Medical School, Tochigi 329-0498, Japan; †Institute of Bioregulation, Kyushu University, Ohita 874-0838, Japan; ‡Transcriptome Profiling Group, National Institute for Radiological Science, Chiba 263-8555, Japan; §Genetics Division, National Cancer Center Research Institute, Tokyo 104-0045, Japan; ¶Faculty of Engineering, Toyama University, Toyama 930-8555, Japan; and ‖Department of Molecular Virology, Immunology, and Medical Genetics, Comprehensive Cancer Center, Ohio State University, Columbus, OH 43210

Contributed by Carlo M. Croce, May 23, 2005

We report the identification and characterization of a potent regulator of genomic integrity, mouse and human *FRAG1* gene, a conserved homolog of replication factor C large subunit that is homologous to the alternative replication factor C subunits Elg1, Ctf18/Chl12, and Rad24 of budding yeast. *FRAG1* was identified in a search for key caretaker genes involved in the regulation of genomic stability under conditions of replicative stress. In response to stress, Atr participates in the down-regulation of *FRAG1* expression, leading to the induction of apoptosis through the release of Rad9 from damaged chromatin during the S phase of the cell cycle, allowing Rad9–Bcl2 association and induction of proapoptotic Bax protein. We propose that the Frag1 signal pathway, by linking replication stress surveillance with apoptosis induction, plays a central role in determining whether DNA damage is compatible with cell survival or whether it requires cell elimination by apoptosis.

genomic integrity | Bcl2 | Rad9 | Atr | Rb

Replicative stress causes replication fork stalling or arrest, which can occur in yeast at naturally occurring sequences, such as replication fork barriers and replication slow zones (1). When damage is severe or the natural order of DNA replication is perturbed, DNA double-strand breaks can occur (2). Such events can trigger cellular checkpoints, allowing time for repair of damage before cell cycle progression (2). When the breaks are fixed or the damage is compatible with cell survival, double-strand breaks can give rise to the fixed chromosomal aberrations observed in cancer cells, such as translocations, inversions, amplifications, and deletions. Accumulated aberrations of caretaker pathways in concert with alterations of gatekeeper tumor suppressors give rise to transformed cells that acquire selective growth and survival advantages (3). Thus, the pathology of stalled or collapsed replication forks is important for understanding the role of faithful regulation of replication in preventing carcinogenesis.

Genotoxic stress-induced replication stalling activates checkpoint-signaling pathways that block cell cycle progression, control DNA repair, or trigger apoptosis (4) through membrane death receptors and the endogenous mitochondrial death pathways (5). Rad9 protein is involved in the control of the DNA damage-induced checkpoint (6). Studies in yeast and human cells have shown that Rad9 interacts with Hus1 and Rad1 in the 9-1-1 complex, which is a heterotrimeric complex and acts as a proliferating cell nuclear antigen-like sliding clamp (4, 7). In response to DNA damage, the 9-1-1 complex is loaded around DNA lesions by Rad17, which binds to chromatin before damage (8) and facilitates Atr-mediated phosphorylation and activation of Chk1 kinase to arrest cell cycle. Rad9 can participate in signaling apoptosis by interacting with antiapoptotic Bcl-2 family proteins Bcl-2 and Bcl-X_L but not with proapoptotic Bax and Bad (9). The interaction of Bcl2 with Bax prevents Bax from inducing cytochrome *c* release and cell death, and the Bax/Bcl2 ratio is crucial for regulation of apoptosis (10). Because the 9-1-1 clamp is also involved in DNA repair (7), the Rad9 complex is thought to play a key role in coordinating multiple functions of checkpoint activation, DNA repair, and apoptosis.

In this study, we report the identification and characterization of the *FRAG1* gene, which encodes a 1,820-aa mouse and 1,844-aa human conserved, uncharacterized protein homolog of the large replication factor C (RFC) subunit Rfc1 (861 aa) and the alternative RFC subunits Elg1 (791 aa), Ctf18/Chl12 (741 aa), and Rad24 (659 aa; Rad17 in human) in budding yeast. Elg1 (enhanced levels of genome instability), a RFC homolog, which forms an alternative RFC complex with Rfc2–Rfc5, was discovered through budding yeast genome-wide synthetic genetic interaction screening of mutants of replication fork-progression genes (11) and through the study of mutants exhibiting high levels of Ty recombination (12, 13). The Elg1 complex is distinct from RFCs for DNA replication, the DNA damage checkpoint, and sister chromatid cohesion (11–14). We have now isolated the mammalian *FRAG1* gene, characterized the function of Frag1 protein in higher eukaryotes, compared it with homologous DNA replication and damage response proteins of simpler organisms, and shown that it is involved in a Rad9-related damage checkpoint, a pathway that is important in determining whether DNA damage will be tolerated or whether the damaged cells will be eliminated by apoptosis.

Materials and Methods

Cell Culture. For synchronization by double thymidine block, after culture in medium with 10% FCS/DMEM containing 2.5 mM thymidine for 24 h (the first block), cells were washed with PBS, grown for 10 h in fresh DMEM/10% FCS, cultured 16 h in 2.5 mM thymidine (the second block) and then incubated as indicated without thymidine. Flow cytometric analysis after BrdUrd incorporation showed that >90% cells entered S phase 2–8 h after release. Cell viability was assessed by visualization of cell morphology, trypan blue, or erythrosine B exclusion, Hoescht 33342 vital staining, and flow-assisted cytometric analysis.

Genotoxic Stress and Colony Assay. For synchronized cells, 0.4 μM aphidicolin (Sigma) in 0.2% DMSO was included in the thymidine medium for 16 h of the second synchronization. Medium was exchanged for thymidine-free medium containing 2.2 μM caffeine (Sigma) and 0.4 μM aphidicolin for an indicated period. For DNA

Abbreviations: MEF, mouse embryonic fibroblast; MMS, methyl methanesulfonate; RFC, replication factor C; siRNA, short interfering RNA.

Data deposition: The sequences reported in this paper have been deposited in the GenBank database (accession nos. AY557610 and AY557611).

**To whom correspondence should be addressed at: Comprehensive Cancer Center, Ohio State University, Wiseman Hall, Room 385L, 410 West 12th Avenue, Columbus, OH 43210. E-mail: carlo.croce@osumc.edu.

damage, the DNA alkylating agent methyl methanesulfonate (MMS) (15) was added in the medium at indicated conditions. For UV irradiation, 60–70% confluent monolayer cells were irradiated with UV-C emitted by germicidal lamps (GL-15, NIPPO Electronic, Tokyo, Japan) emitting at predominantly 254 nm. For colony assay, cells were cultured in medium with MMS for 1 h, washed, and plated in DMEM/10% FBS with 1.5% methylcellulose; colonies were counted 10 days later. For radiation, cells were exposed to ^{137}Cs [661 keV (1 eV = 1.602×10^{-19} J) at indicated doses] and assessed as indicated.

Plasmids and Small Interfering RNAs (siRNAs). pcDNA4V5 DNA (Clontech), was ligated in-frame with F1 (nucleotide positions from the first coding methionine, 1–1440), F2 (1400–1839), F3 (1794–3177), F4 (2697–3975), or FZ (3972–5535) DNA fragments of human Frag1 cDNA. Wild-type pBJF-FLAG-ATR (pBJF-FLAG-ATRwt), kinase-dead pBJF-FLAG-ATR (pBJF-FLAG-ATRkd) [from S. Schreiber (Harvard University, Cambridge, MA) and K. Cimprich (Stanford University, Stanford, CA)], HA-Rad9, Flag–N-terminally deleted Rad9 [Rad9-δN; from H-G. Wang (University of South Florida, Tampa)], and pCAGGS-hbcl-2 [from Y. Eguchi and Y. Tsujimoto (Osaka University, Osaka, Japan)] were used for transfection. GST-fusion (Amersham Pharmacia) was used for protein expression.

Construction of siRNA-expression plasmids was based on the U6 siRNA expression vector (Takara, Mie, Japan), which includes a mouse U6 promoter, a puromycin-resistance gene, and two BspMI sites. Two sets of the sense and antisense oligonucleotides (Table 1, which is published as supporting information on the PNAS web site) were annealed and ligated into the vector. U6 siRNA-Frag1 plasmids were transfected into cells by using TransIT-TKO transfection reagent (Mirus, Madison, WI) and selected in 1 μg/ml puromycin. Colonies were picked, and expression was evaluated by RT-PCR and immunoblot analysis. siRNA expression vectors with EGFP antisense or without inserts were used as controls (Takara). Oligo siRNAs for mouse p73, Atr, and luciferase were used as recommended (Santa Cruz Biotechnology).

cDNA Isolation and RNA Analysis. RNAs were extracted with a Qiagen (Valencia, CA) kit and cDNAs synthesized from 2 μg of poly(A)$^+$ RNA with Superscript II reverse transcriptase and oligo(dT) and random primers (Invitrogen). Differentially expressed genes were isolated with a cDNA subtraction kit (Clontech). After two rounds of hybridizations, cDNAs were amplified, ligated to vector, and sequenced.

For hybridization, 5-μg RNAs were fractionated by agarose gel electrophoresis, transferred to Nylon membrane, and hybridized with the following probes: cDNAs of the peptide coding region of *FRAG1* (N- and C-terminal), *RFC1*, *CTF18*, *DCC*, and *RAD17*, which were amplified by RT-PCR, subcloned, and sequenced. Filters were washed and exposed to x-ray film.

Protein Analysis and Fractionation. For immunoprecipitation, cells were harvested and 500-μg samples of cell lysates, after being precleared with protein G-Sepharose beads, were incubated with 3–4 μg of specific antibody overnight. Antigen–antibody complex was immobilized on protein G-Sepharose beads, and the beads were washed five times in lysis buffer. Bound proteins were eluted by boiling and subjected to SDS/PAGE and immunoblotting. Immunofluorescence staining and confocal analysis were performed by culturing cells in chambered slides, followed by methanol fixation, 0.05% Triton X-100 treatment, and staining with first and secondary antibodies. Primary antibodies used were anti-human p53 (BD Biosciences), phosphorylated p53 (Ser-15) (BD Biosciences), Mdm2 (Santa Cruz Biotechnology), Rb (BD Biosciences), Rad9 (Santa Cruz Biotechnology), phospho-H2AX (catalog no. 07-164; Upstate Biotechnology, Chicago), mitochondria (Chemicon), Bax (catalog no. 2772, Cell Signaling Technology; N-20, Santa Cruz Biotechnology), Atr (ab-2, EMD Biosciences, San Diego; catalog no. sc-1887, Santa Cruz Biotechnology), Orc2 (BD Biosciences), cytochrome *c* (Pharmingen), phospho-H2AX (catalog no. 05-636; Upstate Biotechnology), Grb2 (BD Biosciences), V5 (Invitrogen), Flag (Sigma), and actin (ICN, Irvine CA), which were detected with secondary antisera in an enhanced chemiluminescence system (ECL, Amersham Biosciences). Rabbit polyclonal anti-Frag1 antiserum was developed against peptide sequences mouse 345 CSLSDPENEQPVQKRKSN 362 and affinity-purified. *In vitro* transcription/translation was performed with a rabbit reticulocyte system (Amersham Biosciences) by labeling cDNAs cloned by RT-PCR amplification with [^{35}S]methionine (Amersham Biosciences). Proteins were incubated in 100 μl of binding buffer containing 150 mM NaCl, 0.1% Tween 20, 0.75 mg/ml BSA, 50 mM Tris·HCl (pH 8.0), 5 mM EDTA, and 10% (vol/vol) glycerol. For pulling down, glutathione–agarose bead-bound proteins were subjected to SDS/PAGE after being washed five times, and the gels were exposed to x-ray film. Cellular fractions were prepared as described in ref. 16.

Results and Discussion

Identification of FRAG1, a Gene Differentially Expressed After Replication Stress. DNA replication guarantees the duplication of the genome and requires concerted, dynamic changes of expression of specific gene products, which regulate the integrity of replication and surveillance of the genome for damage (17). When replication forks encounter damage in the DNA strands, stalling or arrest can result, leading to stimulation of the downstream checkpoint to initiate cell cycle arrest or apoptosis (1); however, the molecular mechanisms that sense stalled replication are not understood fully. To study differentially expressed genes in conditions of replication stress, synchronized mouse embryonic fibroblasts (MEFs) were exposed to aphidicolin, a DNA polymerase inhibitor, and harvested 4 h (in mid-S phase) after release from a double thymidine block. RNA was extracted from MEFs, and subtractive cDNA hybridization was performed to identify genes differentially expressed in the presence or absence of aphidicolin (Fig. 7*A*, which is published as supporting information on the PNAS web site). BLAST database searches indicated that 155 clones that we isolated and sequenced included 86 clones (55%) identical to mouse ESTs (>95% homologous over 200 bp). The 86 clones included redundant clones; 13 clones corresponded to an overlapped cDNA contig (denoted as FRAG1/N), seven clones corresponded to a contig (FRAG1/C), and five clones corresponded to *RFC1* cDNA. Interestingly, database searches indicated that FRAG1/N and FRAG1/C are located adjacent to each other (C130052G03Rik, GenBank accession no. XM_282980; Gm17, GenBank accession no. XM_111221) on mouse chromosome 11. Database searches for human orthologs of the mouse clones showed that the orthologs are parts of a continuous gene, FLJ12735 (GenBank accession no. NM_024857), at human chromosome 17q11.2. RT-PCR amplification indicated that those "two" mouse transcripts span a gene, suggesting that the two transcripts, FRAG1/N and FRAG1/C came from one gene, *FRAG1* (Ctf18/Rad24/Elg1-related gene 1). We have focused on characterization of the *FRAG1* gene.

Alteration of FRAG1 Expression. Northern blot analysis was performed with replication-related genes *RFC1*, *RAD17*, and *CTF18*, as well as FRAG1/N and FRAG1/C as probes. Synchronized MEFs were treated with aphidicolin or MMS (a DNA alkylating agent), agents that cause stalled DNA replication (15). Expression of FRAG1/N and FRAG1/C was markedly down-regulated by aphidicolin or MMS treatment, whereas the effect on *RFC1*, *Rad17*, and *CTF18* genes was less apparent after MMS treatment (Fig. 1*A*). RNA blot with cDNA probes of N- and C-terminal portions of *FRAG1* (FRAG1/N and FRAG1/C) (Fig. 1*C*) detected a predominant transcript of ≈9 kb expressed ubiquitously in 12 murine cell lines (Fig. 1*B*). To assess the stability of the *FRAG1* transcript,

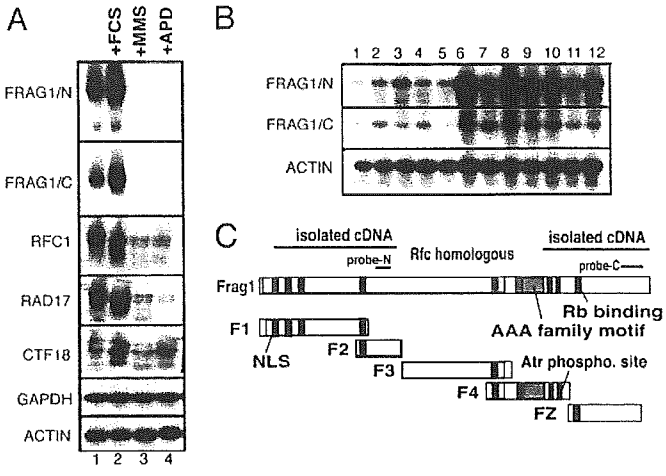

Fig. 1. Expression of the *FRAG1* gene. (*A*) RNA blot analysis. Synchronized MEFs were treated with aphidicolin, and 20 μg of each of the total RNAs were loaded on the gel, transferred to membrane, and hybridized to probes as indicated. (*B*) Frag1 expression in various mouse cell lines. Shown are poly(A)$^+$ RNA from the following sources: lane 1, PU5–1.8 (lymphoid tumor); lane 2, RAW264.7 (leukemia-virus induced tumor); lane 3, K-BALB (Kirsten murine leukemia virus-transformed fibroblast); lane 4, 3T3 (fibroblast); lane 5, L-M (murine L cells, transformed adipose connective tissue); lane 6, P19 (teratocarcinoma); lane 7, Hepa 1-6 (hepatoma); lane 8, R1.1 (T cell lymphoma); lane 9, L1210 (lymphocytic leukemia); lane 10, P388D1 (lymphoma); lane 11, P815 (mastcytoma); and lane 12, NB41A3 (neuroblastoma). (*C*) A map of Frag1 fragments. F1, F2, F3, F4, and FZ are cDNA fragments used in the study. Location of probes Frag1/N and Frag1/C in the cDNA are indicated. Rb binding motif LxCxE and two putative Atr-phosphorylation sites are located near a region homologous to the AAA family. Two locations of cDNA fragments, which were isolated through subtractive hybridization (nucleotide positions from the first methionine, 321–1835 and 3750–5388) are shown, and two probes for RNA blot analysis, which were synthesized by PCR amplification (nucleotide positions from the first methionine, 1580–1830 and 5130–5380) are shown. NLS, nuclear localization motifs.

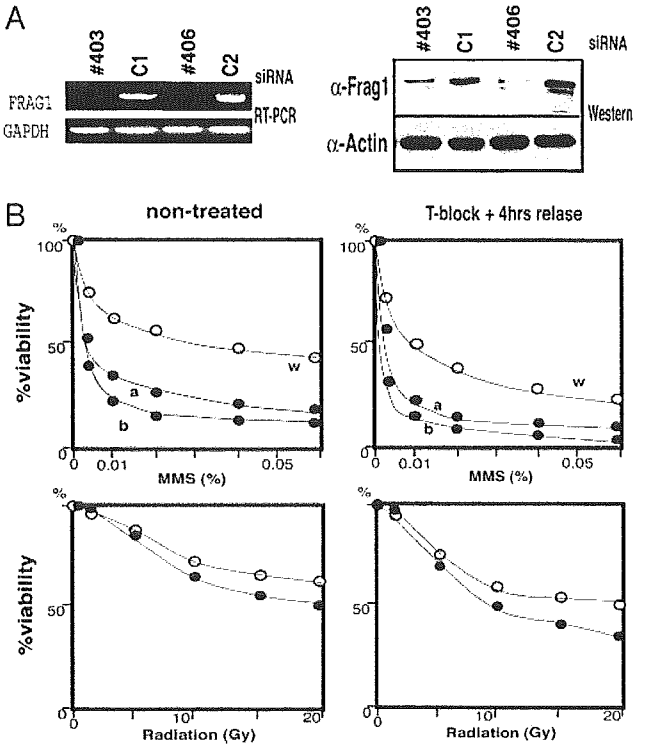

Fig. 2. Down-regulation of Frag1 expression sensitizes cells to replicative stress. (*A*) Down-regulation of *FRAG1* by siRNA. MEFs were transfected by U6 siRNA expression vector against FRAG1 and grown in selective medium. RNAs and protein lysates were extracted and analyzed by RT-PCR and immunoblot. Results of two independent experiments of *FRAG1* siRNA clones (#403 and #406) are shown. C, mock control siRNA. (*B*) Colony survival assay after exposure to MMS. Synchronized (*Right*) or asynchronized (*Left*) cells (1×10^6) were cultured in thymidine-free medium for 2 h to allow S-phase entrance. (*Upper*) MMS was added at the indicated concentrations for an additional 1 h, and cells were washed. (*Lower*) For radiation, cells were exposed at the indicated doses. Cells were plated in DMEM containing 1.5% methylcellulose, and colonies were counted 10 days after treatment. The percentage of survival was determined relative to the numbers of colonies from untreated cells. Lines labeled a and b indicate experiments with two independent siRNAs; lines labeled w indicate mock.

cells treated with actinomycin D to inhibit *de novo* RNA synthesis in medium with or without aphidicolin were harvested at serial time points and assessed for *FRAG1/N*, *FRAG1/C*, *CTF18*, *RFC*, and *RAD17* mRNA, indicating that the half-life of *FRAG1* mRNA appears to be <4 h after exposure to aphidicolin. In contrast, the half-life of *CTF18*, *RFC*, and *RAD17* mRNAs was >15 h, suggesting that *FRAG1* mRNA appeared less stable than transcripts of the other replication-related genes examined (Fig. 7 *B–E*).

Database searches indicated that the putative Frag1 protein has a conserved region homologous to a large subunit of RFC, which is considered an ortholog of the alternative RFC subunits, Elg1, Ctf18/Chl12, and Rad24 (Rad17 in fission yeast and human) of budding yeast (Fig. 1*C*) (11–14). Frag1 has a conserved AAA family motif, a hallmark of the ATPase family associated with various cellular activities, including chaperone-like functions that assist in the assembly, operation, or disassembly of protein complexes. Comparison of the mouse and human Frag1 amino acid sequences indicated that they conserve putative Atr-phosphorylation sites (mouse Frag1 at Ser-1150 and Ser-1168 and human Frag1 at Ser-1169 and Ser-1187) (18, 19), and a putative Rb binding site with a Leu-x-Cys-x-Glu (LxCxE) motif (amino acids 1409–1413 of mouse and 1428–1432 of human) (20).

Reduction of Frag1 Protein Increases Sensitivity to DNA Damage. Studies of budding yeast have shown that elg1Δ mutants are sensitive to DNA damage, suggesting that Elg1-RFC functions in the DNA damage response (11, 12). To study the effect of reduced expression of mammalian Frag1 protein, we performed siRNA experiments to inhibit expression of endogenous Frag1. RT-PCR and immunoblot study showed that cells transfected with the siRNA vector and selected in puromycin medium showed a marked reduction of Frag1 gene product (Fig. 2*A*). *FRAG1* siRNA transfectants were exposed to MMS or to γ-irradiation, and colony survival was assayed. Compared with control siRNA transfectants, two independent *FRAG1* siRNA transfectants showed enhanced sensitivity to replication stress, which was apparent in synchronized MEFs, suggesting that the damage activated the S phase checkpoint (Fig. 2*B*). The difference between siRNA knock-down and control cells after MMS treatment is more pronounced than differences observed after γ-irradiation. It is suggested that reduction of Frag1 increased the sensitivity to MMS.

Frag1 siRNA Inhibition Leads to Activation of Caspase and BAX. Immuunoblot analysis of Frag1 protein expression showed that Frag1 was reduced 2–6 h after exposure to aphidicolin or MMS, a reduction more rapid than for actin or Rad17 in MMS (Fig. 3*A*). Because involvement of Frag1 in cellular responses to DNA damage is suggested, we assessed the activation of proapoptotic proteins. Immunoblot analysis showed caspase 7 activation in *FRAG1* siRNA transfectants but not in control siRNA transfectants (Fig. 8*A*, which is published as supporting information on the PNAS web site). Bax protein expression with slow mobility was induced in two independent *FRAG1* siRNA transfectants 8 h after release from double thymidine cell cycle block and was markedly induced in

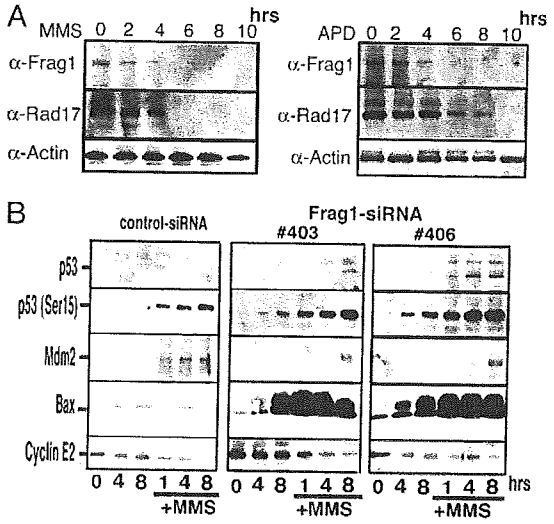

Fig. 3. Frag1 is involved in genotoxic response. (*A*) Frag1 down-regulation by genotoxic stress. MEFs were cultured in medium with 0.4 nM aphidicolin or 0.01% MMS for the indicated times. Cells were harvested, and lysates were subjected to SDS/PAGE and immunoblot analysis with antisera as indicated. (*B*) Frag1 knock-down sensitizes cells to genotoxic stress. Two independent Frag1 siRNA MEF clones (#403 and #406) synchronized in G_1 and grown in thymidine-free medium with or without exposure to MMS were harvested at the indicated times after release in thymidine-free medium. Protein lysates were immunoblotted with antibodies as indicated. Mismatched siRNA served as control.

those *FRAG1* siRNA transfectants at all times after MMS exposure. In sharp contrast, Bax induction was not apparent in control siRNA transfectants in the conditions examined (Fig. 3*B*).

Upon activation by DNA damage-induced or oncogene-induced signaling pathways, phosphorylation of p53 at Ser-15 increases its half-life, accumulation, and tumor suppressing activity (21). Phosphorylation of p53 at Ser-15 leads to reduced interaction of p53 with its negative regulator, the oncoprotein Mdm2, and impairs the ability of Mdm2 to inhibit p53-dependent transactivation (21). Our analysis of two independent Frag1 siRNA transfectants showed that phosphorylation of p53 at Ser-15 was induced in cells after MMS exposure and at 4 (Fig. 3*B*, #406) and 8 h (Fig. 3*B*, #403 and #406) without MMS. In control siRNA transfectants, phosphorylation of p53 at Ser-15 was induced in cells after, but not before, exposure to MMS, showing that, even without MMS, the reduction of Frag1 can stimulate Bax induction in synchronized cells (at 4 or 8 h), emphasizing that reduction of Frag1 sensitizes cells to genotoxic response. Alteration of Mdm2 expression was less apparent. Taken together with the observation by microscopy that cytochrome *c* was released from mitochondria when Frag1 expression was inhibited by siRNA or when cells were exposed to MMS (Fig. 8*C*), it is suggested that reduction of Frag1 may be required for sensitizing cells to DNA damage and activating Bax-related cell death.

p53 translocates to mitochondria, where it directly induces Bax activation and cytochrome *c* release upon DNA damage (22). To determine whether p53 is involved in the induction of Bax expression in our siRNA transfectants, Trp-53-deficient MEFs were analyzed. Results of siRNA Frag1 inhibition showed that Bax was induced in Trp-$53^{+/-}$ and Trp-$53^{-/-}$ transfectants of MEFs and phosphorylation of p53 at Ser-15 was increased in Trp-$53^{+/-}$ transfectants after exposure to MMS, suggesting that Bax was activated regardless of p53 status and that p53 is dispensable for Bax induction in the Frag1 replication stress pathway (Fig. 8*B*). Recently, two p53 homologues have been identified, p73 and p63, that have high amino acid identity, suggesting shared function (23).

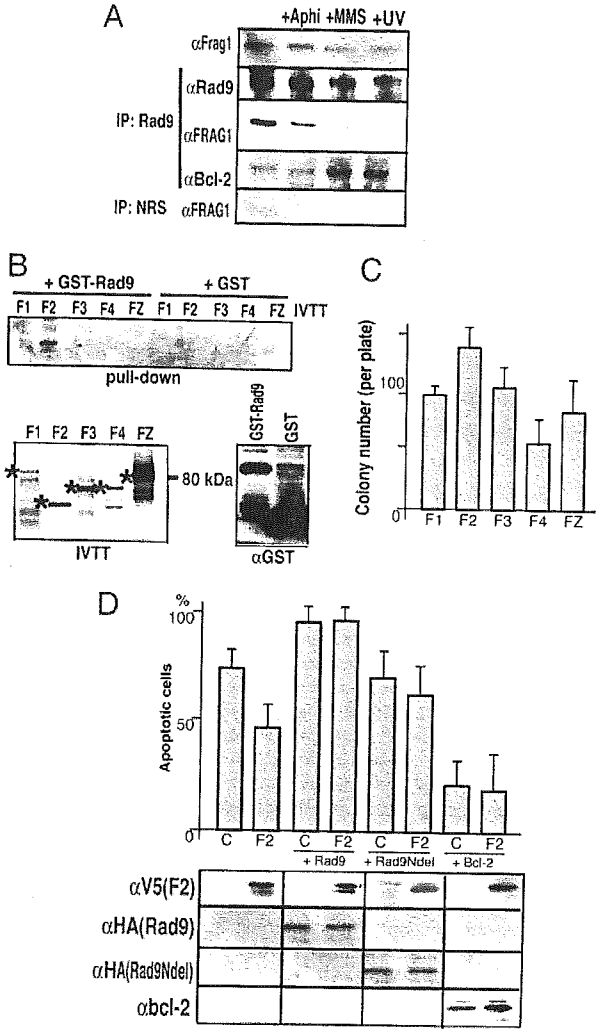

Fig. 4. Frag1 is involved in the Rad9–Bcl2 pathway. (*A*) Coimmunoprecipitation of Frag1, Rad9, and Bcl2. MEFs were grown in medium with 0.4 μM aphidicolin (Aphi) or 0.01% MMS for 24 h or exposed to 8 J/m^2 UV radiation and cultured for 24 h before harvesting. The leftmost lane is without treatment. Protein lysates were extracted and immunoprecipitated (IP) with anti-Rad9 or normal rabbit serum (NRS), followed by immunoblot with Frag1, Rad9, or Bcl2 antisera. (*B*) Pull down of *in vitro* transcribed and translated (IVTT) F1, F2, F3, F4, and FZ fragments of Frag1 by GST–Rad9 fusion protein. *In vitro* transcribed and translated products were labeled with [^{35}S]methionine and incubated with GST–Rad9 fusion protein. The bound samples were pulled down with glutathione-agarose beads, which were subjected to SDS/PAGE, and gels were exposed to x-ray film. (*Upper*) Pull-down assay. (*Lower Left*) PAGE and exposure of *in vitro* transcribed and translated F1, F2, F3, F4, and FZ fragments (input), shown by asterisks. (*Lower Right*) Immunoblot with anti-GST. (*C*) Assay of colony survival of MEF transfectants after MMS exposure. MEFs transfected with pcDNA expression vector with F1, F2, F3, F4, or FZ cDNA and selected in G418 medium were subjected to colony survival assay, similarly to that shown in Fig. 2*B*. Error bars show standard deviations. (*D*) Cell death after MMS exposure. (*Upper*) Rad9, Rad9-δN (Rad9Ndel), and Bcl2 plasmids were introduced with selection plasmids in F2 transfectants and grown in selection medium for hygromycin resistance. Apoptotic cells were evaluated 48 h after MMS exposure by erythrosine B staining exclusion. (*Lower*) Immunoblot with anti-V5 tag (F2), anti-HA tag (Rad9), anti-HA tag (Rad9Ndel), and anti-Bcl2 antisera.

Indeed, like p53, p73 can trigger several promoters, including Bax and p21 promoters, and is able to trigger cell death in response to the DNA damage. Introduction of p73 oligo siRNA into Frag1 siRNA vector transfectants of Trp-$53^{-/-}$, reduced Bax induction (data not shown), suggesting a role for p73 in the stimulation of the Frag1—Bax pathway.

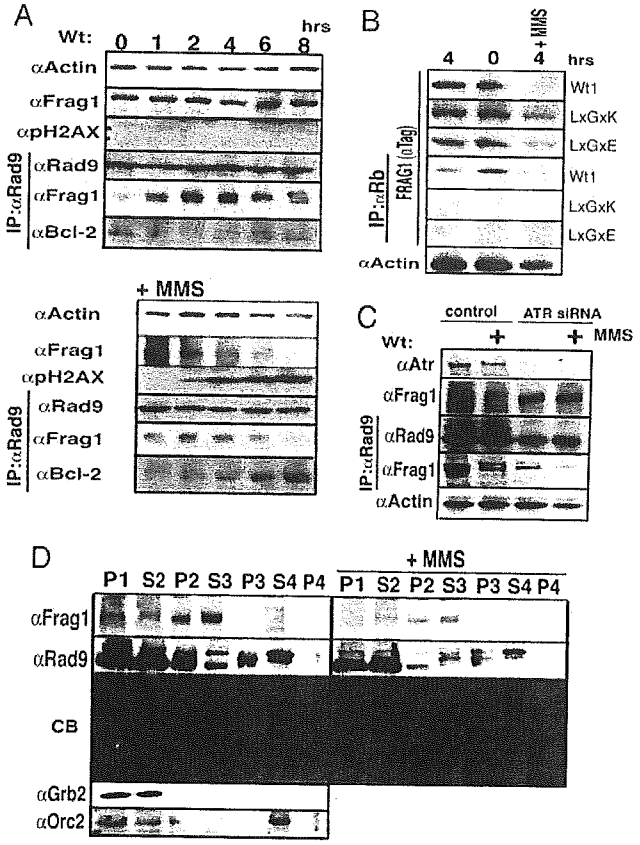

Fig. 5. Frag1 involvement in the DNA damage response. (*A*) Synchronized MEFs were cultured in growth medium with or without MMS (0.01%) for the indicated times, and cellular protein was extracted. Protein expression was studied by immunoblot with the indicated antibodies before and after immunoprecipitation (IP) with Rad9 antibody. (*B*) LxGxK, LxGxE, or wild-type (Wt) Frag1 transfectants that were synchronized at G_1 were released from G_1 in thymidine-free medium with or without MMS (0.01%) as indicated and subjected to immunoblot with anti-V5 (tag) or anti-actin antibody before and after immunoprecipitation with Rb antibody. (*C*) MEFs were transfected with Atr siRNA. A day after transfection, cells were cultured with or without MMS (0.01%) for 4 h, and protein lysates were immunoprecipitated and immunoblotted as indicated. (*D*) Subcellular localization of Frag1 and Rad9 after MMS treatment. Cellular components were fractionated from MEFs before and after exposure to MMS and subjected to immunoblot. Immunoblot with antibodies against Grb2 and Orc2, membranous and chromatin-bound proteins, are shown as controls. P1, whole-cell pellet; S2, cytosol and nucleosol; P2, detergent-insoluble nuclei; S3, DNase I-extracted nuclei; P3, DNase I-resistant fraction; S4, containing chromatin; P4, nuclear matrix. CB, Coomassie brilliant blue staining.

Frag1 Associates with Rad9 and Is Involved in the Bcl2 Pathway. It was shown that proapoptotic Bax can form heterodimers with antiapoptotic Bcl2 in cells (24), which prevents Bax conformational changes required for apoptosis induction (10). Activated Bax proteins oligomerize and are stabilized in the mitochondrial membrane and induce cytochrome *c* release, an important process for the induction of cell death (10). After DNA damage, Rad9 plays a role in induction of apoptosis by associating with antiapoptotic Bcl2, which results in the inhibition of Bcl2 function (9). To investigate the Frag1 signal pathway, we have used coimmunoprecipitation analyses (Fig. 9*A*, which is published as supporting information on the PNAS web site) to define Frag1 associations with partner proteins involved in responses to replicative stress. Immunoblots probed with anti-Frag1 after immunoprecipitation with anti-Rad9 indicated their association in growing cells. Aphidicolin or MMS exposure resulted in reduced Frag1 expression and concomitant

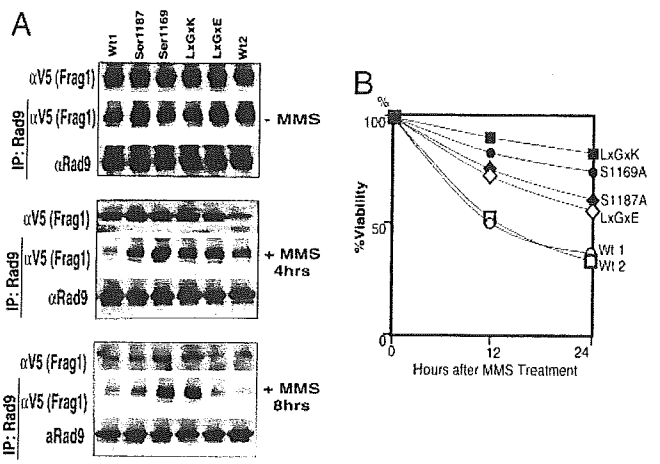

Fig. 6. The Frag1 response to DNA damage. (*A*) Association of Frag1 and Rad9 in response to DNA damage. Wild-type (Wt) and Frag1 mutant MEF transfectants synchronized at G_1 were released from G_1 in thymidine-free medium with 0.01% MMS for 4 or 8 h. Cellular lysates were extracted and subjected to immunoblot with anti-V5 (tag) or anti-actin antibody before and after immunoprecipitation (IP) with Rb antibody. (*B*) Viability of cells expressing wild-type and Frag1 mutants after MMS exposure. Wild-type and Frag1 mutant-expressing MEFs were cultured in medium with 0.01% MMS for the indicated times, and apoptotic cells were evaluated by erythrosine B staining exclusion.

reduction of the association with Rad9. Conversely, an increase of Rad9 association with Bcl2 was observed after genotoxic stress (Fig. 4*A*). *In vitro* pull-down assay using recombinant GST–Rad9 fusion protein detected association with *in vitro* transcribed–translated Frag1-F2 fragment, corresponding to the RFC homologous region. Other Frag1 fragments did not associate with Rad9 (Figs. 1*C* and 4*B*), suggesting that the F2 fragment binds Rad9 and regulates apoptosis induction.

Colony formation assays of MEF transfectants expressing specific Frag1 peptides indicated that more colonies formed after F2 expression compared with other Frag1 peptides after genotoxic stress (Fig. 4*C*), suggesting that the F2 region of Frag1 functions to regulate apoptosis by interacting with Rad9. The stable F2 transfectants, in which MMS-induced apoptosis was inhibited, were transfected with Rad9 and selected for hygromycin resistance (Fig. 4*D Upper*, compare F2 and C). Overexpression of Rad9 in the F2 expressors caused an increase in apoptosis (Fig. 4*D*, +RAD9). Usage of Rad9-δN, which is defective in Bcl2 association (9), inhibited apoptosis (Fig. 4*D*, +Rad9Ndel). Furthermore, introduction of antiapoptotic Bcl2 into F2 transfectants resulted in profound inhibition of apoptosis (+Bcl2). Confocal microscopy showed that in F2 transfectants release of cytochrome *c* after exposure to MMS was inhibited (Fig. 9*B*). Results of these experiments strongly suggest that Frag1 modulates Rad9 association with Bcl2 and thereby induces DNA damage-induced apoptosis.

Atr Regulates Frag1–Rad9 Association and the Release of Rad9 from Frag1 in S Phase. To further define Frag1 function, we examined the cell cycle-dependence of Frag1 association with Rad9 in synchronized cells exposed to MMS. Association of Frag1 with Rad9 was weak in synchronized G_1 cells and increased in strength during progression into S phase. After exposure to MMS, the Frag1–Rad9 association was reduced, leading to an increase of Rad9–Bcl2 association (Fig. 5*A*). The data are consistent with the conclusion that Frag1 is involved in sensitizing Rad9 to genotoxic stress during S phase through their association. Confocal microscopic observation indicated that Frag1 and Atr are colocalized 8–12 h after exposure to MMS, whereas Frag1 seems to form foci before Atr focus formation (Fig. 10, which is published as supporting infor-

mation on the PNAS web site), suggesting a role for Frag1 in the Rad9 pathway via Atr response to DNA damage.

To study further the involvement suggested by the Frag1 motif search (Fig. 1*C*) of Atr and Rb in the Frag1–Rad9 pathway, we prepared wild-type and mutant human Frag1 expression vectors by substituting the putative Atr phosphorylation sites, Ser-1169 and Ser-1187 with Ala residues, and the Rb-binding site, LxCxE-1432 with LxGxK-1432 or LxGxE-1432. Transfected wild-type Frag1, but not LxGxE and LxGxK mutants, associated with Rb, as was more apparent in synchronized G_1 than S phase cells (Fig. 5*B*). After MMS, wild-type Frag1 expression was undetectable, whereas LxGxK, and to a lesser extent LxGxE, mutant proteins were detectable. The Frag1–Rb association was undetectable in wild type and two Rb-site mutants after MMS. In summary, it is suggested that Frag1 might play a role in pre-sensitizing cells to genotoxic stress during replication, i.e., in S phase, whereas Frag1 predominantly associates with Rb in G_1 phase.

To examine the role of Atr, endogenous Atr was inhibited by siRNA (Fig. 5*C*). Whereas MMS damage reduced endogenous Frag1 in control cells, reduction of Atr inhibited the down-regulation of endogenous Frag1 in response to DNA damage. Immunoprecipitation showed that, in response to MMS exposure, inhibition of Atr markedly reduced the association of Rad9 with Frag1, a reduction in siRNA ATR-treated cells that was more appreciable than in control cells. Thus, Atr stimulated two separable events: association of Rad9 with Frag1 and down-regulation of Frag1 in response to DNA damage.

Cellular components before and after MMS exposure were fractionated, and proteins were analyzed by immunoblot to study the translocation of Rad9 in response to DNA damage (Fig. 5*D*). After exposure to MMS, the amount of Rad9 in detergent-insoluble nuclei (P2) was significantly reduced, and the proportion of slow mobility Rad9 was increased in DNase I-extracted nuclei (S3), whereas reduction but not translocation of Frag1 was detected, suggesting that a predominant fraction of Rad9 translocated from chromatin to soluble fraction. These results suggest that Frag1 has a role in loading activated Rad9 onto damaged chromatin and stimulating its translocation.

To determine whether phosphorylation and Rb-binding of Frag1 are involved in the association and release of Rad9 (Fig. 6*A*), stable transfectants expressing Frag1 or Frag1 mutants were exposed to MMS, and protein lysates were analyzed by immunoblot. Association of Frag1 with Rad9 was reduced 4 and 8 h after cells were released from G_1 block and exposed to MMS; however, the reduction was inhibited in the Ser-1169A and LxGxK mutants and, to a lesser extent, in Ser-1187A and LxGxE mutants, suggesting that Atr phosphorylation stimulates the dissociation of Rad9 and that Rb binding is also involved, directly or indirectly, in Rad9 activation. The evaluation of apoptotic cells showed that the mutants, especially Ser-1169A and LxGxK, had DNA damage-resistant phenotypes compared with wild-type transfectants (Fig. 6*B*), emphasizing the importance of the Frag1–Rad9 association to apoptosis induction. We finally assessed cotransfectants with Frag1 and wild-type or kinase-dead ATR. Immunoblot analysis showed that, after MMS exposure, down-regulation of Frag1 was inhibited by kinase-dead ATR but not by wild-type ATR (data not shown), supporting the conclusion that phosphorylation by Atr plays a role in the Frag1–Rad9-regulated DNA damage response.

As for a mechanism, our data showed that Frag1 amino acids Ser-1169 and Ser-1187 play critical roles in the regulation of Rad9 release and cell death in response to DNA damage. Ser-1169 and Ser-1187 are putative phosphorylation sites for Atr, which is a sensor of stalled or collapsed replication forks at mid-S phase checkpoint (19). Overexpression of a Rad9-associated Frag1 polypeptide inhibited Bcl2 family-mediated apoptosis, suggesting that Frag1 functions as a platform for loading Rad9 to damaged lesions. As shown in the present study of *ATR* siRNA, after genotoxin exposure, reduction of Atr inhibited the down-regulation of endogenous Frag1 and markedly reduced association of Rad9 with Frag1, suggesting that the loading of Rad9 onto damaged chromatin by Frag1 may require Atr and that Atr could down-regulate Frag1 through phosphorylation sites Ser-1169 and Ser-1187. As for the activation of Rad9, earlier studies showed several mechanisms for recruiting Rad9 to damaged lesions, including Abl-mediated phosphorylation of Rad9, which induced binding of Rad9 to antiapototic BclxL (25); PKCδ phosphorylation of Rad9 after genotoxin exposure (26); and MEC1 and TEL1 of budding yeast, homologues of Atr and Atm, which regulate Rad9 hyperphosphorylation (27). Thus, Atr, in concert with those molecules, can play a direct or indirect role in recruiting Rad9 onto Frag1. Full execution of the steps could lead to the stimulation of the Rad9–Bcl2 cell death pathway. We propose a schema in which each step participates in sensing damage, activating checkpoint, and execution of apoptosis; the multisteps may compose the machinery for the pathway, which determines the fate of cells with perturbations in DNA replication progression, i.e., whether the DNA damage is compatible with cell survival or requires elimination by apoptosis (Fig. 11, which is published as supporting information on the PNAS web site).

We thank Drs. Stuart Schreiber and Karlene Cimprich for kindly providing the plasmids pBJF-ATRwt and pBJF-ATRkd, Drs. Yutaka Eguchi and Yoshihide Tsujimoto for kindly providing pCAGGS-hbcl-2, and Dr. Hong Gang Wang for HA-Rad9 and Flag-Rad9-δN. This work was supported in part by research funds from the High-Tech Research Center Project of the Ministry of Education, Culture, Sports, Science and Technology of Japan, the Mochida Memorial Foundation, and the Cell Science Research Foundation.

1. Rothstein, R., Michel, B. & Gangloff, S. (2000) *Genes Dev.* **14,** 1–10.
2. Bakkenist, C. J. & Kastan, M. B. (2004) *Cell* **118,** 9–17.
3. Levitt, N. C. & Hickson, I. D. (2002) *Trends Mol. Med.* **8,** 179–186.
4. Parrilla-Castellar, E. R., Arlander, S. J. & Karnitz, L. (2004) *DNA Repair* **3,** 1009–1014.
5. Kaina, B. (2003) *Biochem. Pharmacol.* **66,** 1547–1554.
6. Dang, T., Bao, S. & Wang, X. F. (2005) *Genes Cells* **10,** 287–295.
7. Hang, H. & Lieberman, H. B. (2000) *Genomics* **65,** 24–33.
8. Zou, L., Cortez, D. & Elledge, S. J. (2002) *Genes Dev.* **16,** 198–208.
9. Komatsu, K., Miyashita, T., Hang, H., Hopkins, K. M., Zheng, W., Cuddeback, S., Yamada, M., Lieberman, H. B. & Wang, H. G. (2000) *Nat. Cell Biol.* **2,** 1–6.
10. Kirkin, V., Joos, S. & Zornig, M. (2004) *Biochim. Biophys. Acta* **1644,** 229–249.
11. Bellaoui, M., Chang, M., Ou, J., Xu, H., Boone, C. & Brown, G. W. (2003) *EMBO J.* **22,** 4304–4313.
12. Ben-Aroya, S., Koren, A., Liefshitz, B., Steinlauf, R. & Kupiec, M. (2003) *Proc. Natl. Acad. Sci. USA* **100,** 9906–9911.
13. Kanellis, P., Agyei, R. & Durocher, D. (2003) *Curr. Biol.* **13,** 1583–1595.
14. Smolikov, S., Mazor, Y. & Krauskopf, A. (2004) *Proc. Natl. Acad. Sci. USA* **101,** 1656–1661.
15. Merrick, C. J., Jackson, D. & Diffley, J. F. (2004) *J. Biol. Chem.* **279,** 20067–20075.
16. Montes de Oca, R., Andreassen, P. R., Margossian, S. P., Gregory, R. C., Taniguchi, T., Wang, X., Houghtaling, S., Grompe, M. & D'Andrea, A. D. (2005) *Blood* **105,** 1003–1009.
17. Bell, S. P. & Dutta, A. (2002) *Annu. Rev. Biochem.* **71,** 333–374.
18. O'Neill, T., Dwyer, A. J., Ziv, Y., Chan, D. W., Lees-Miller, S. P., Abraham, R. H., Lai, J. H., Hill, D., Shiloh, Y., Cantley, L. C., *et al.* (2000) *J. Biol. Chem.* **275,** 22719–22727.
19. Abraham, R. T. (2001) *Genes Dev.* **15,** 2177–2196.
20. Pennaneach, V., Salles-Passador, I., Munshi, A., Brickner, H., Regazzoni, K., Dick, F., Dyson, N., Chen, T. T., Wang, J. Y., Fotedar, R., *et al.* (2001) *Mol. Cell.* **7,** 715–727.
21. Shieh, S. Y., Ikeda, M., Taya, Y. & Prives, C. (1997) *Cell* **91,** 325–334.
22. Chipuk, J. E., Kuwana, T., Bouchier-Hayes, L., Droin, N. M., Newmeyer, D. D., Schuler, M. & Green, D. R. (2004) *Science* **303,** 1010–1014.
23. De Laurenzi, V. & Melino, G. (2000) *Ann. N.Y. Acad. Sci.* **926,** 90–100.
24. Oltvai, Z. N., Milliman, C. L. & Korsmeyer, S. J. (1993) *Cell* **74,** 609–619.
25. Yoshida, K., Komatsu, K., Wang, H. G. & Kufe, D. (2002) *Mol. Cell. Biol.* **22,** 3292–3300.
26. Yoshida, K., Wang, H. G., Miki, Y. & Kufe, D. (2003) *EMBO J.* **22,** 1431–1441.
27. Vialard, J. E., Gilbert, C. S., Green, C. M. & Lowndes, N. F. (1998) *EMBO J.* **17,** 5679–5688.

Available online at www.sciencedirect.com
SCIENCE DIRECT®
Biochemical and Biophysical Research Communications 329 (2005) 288–295
BBRC
www.elsevier.com/locate/ybbrc

Development of new inbred transgenic strains of rats with LacZ or GFP

Hirokazu Inoue [a,1], Ichiro Ohsawa [a,1], Takashi Murakami [a,*], Atsushi Kimura [a], Yoji Hakamata [a], Yuki Sato [a], Takashi Kaneko [a], Masafumi Takahashi [a], Takashi Okada [b], Keiya Ozawa [b], Jeremy Francis [c], Paola Leone [c], Eiji Kobayashi [a]

[a] *Division of Organ Replacement Research, Center for Molecular Medicine, Jichi Medical School, Tochigi 329-0498, Japan*
[b] *Division of Genetic Therapeutics Center for Molecular Medicine, Jichi Medical School, Tochigi 329-0498, Japan*
[c] *Cell and Gene Therapy Center, University of Medicine and Dentistry of New Jersey, Robert Wood Johnson Medical School, NJ 08103, USA*

Received 11 January 2005

Abstract

The ideal goal of regeneration medicine is to restore form and function to damaged tissues. While stem cell transplantation is considered a promising therapeutic approach, knowing the fate of transplanted cells using appropriate markers is essential. We developed new inbred transgenic rat strains with lacZ and GFP based on the transgenic (Tg) animal technique in rats. These Tg animals expressed most of their marker genes ubiquitously, compared to previous Tg rats. Immunological antigenicity against marker proteins was evaluated using conventional skin grafting, and results suggested lacZ-Tg-derived skin was much less immunogenic than that of GFP-Tg. However, GFP-positive cells from parental transgenic rats were still potential candidates for the study of cellular fate in immune privilege sites, such as the brain. Taking advantage of less immunogenic lacZ, we also examined the role of bone marrow-derived cells (BMDCs) in skin wound healing using an in vivo biological imaging system. Although transplantation of BMDCs enhanced wound healing at the injection site, BMDCs were detected only for a short time, suggesting a transient contribution of autologous BMDC-transplantation in wound healing. Our Tg-rat system may provide great benefits for the elucidation of the cellular process of regenerative medicine, including cell and tissue transplantation.

Keywords: Transgenic rat; LacZ; GFP; Immunogenicity; Regenerative medicine; Cellular trafficking

To restore form and function to damaged tissues, a cell and/or tissue transplantation strategy has emerged as a potential therapeutic approach involving the use of autologous cells [1–3]. To examine the fate of the transplanted cells, however, appropriate and stable marking is required for visualization. While it is easy to use fluorescent dye, there is a drawback in that fluorescent intensity decreases during in vivo cellular proliferation. Based on the genetic engineering technique used in rodents [4–7], it is possible to express stable reporter proteins such as β-galactosidase (LacZ) and green fluorescent protein (GFP) in rats and mice. Cells from transgenic animals that express marker genes provide potential benefits for the stable visualization of cellular fate.

We previously developed lacZ- and GFP-Tg rats on a different genetic background, and demonstrated that these Tg rats were suitable for the monitoring of cellular fate in certain experiments [4,5]. However, these Tg animals have a few weak points: all of the tissues did not express enough marker genes in the established animal lines, although both reporter genes were driven under a ubiquitous CMV enhancer/chicken β-actin promoter (CAG promoter) [8]. Furthermore, transplanted cells

* Corresponding author. Fax: +81 285 44 5365.
E-mail address: takmu@jichi.ac.jp (T. Murakami).
[1] These authors contributed equally to this work.

0006-291X/$ - see front matter © 2005 Elsevier Inc. All rights reserved.
doi:10.1016/j.bbrc.2005.01.132

or tissues were occasionally rejected by immune responses due to a mismatch of the minor histocompatibility complex (mHC) derived from an outbred strain of Wistar rats [4]. Herein we redeveloped both lacZ- and GFP-expressing Lewis rats harboring the same genetic background (MHC haplotype: $RT1^l$). These Tg animals express most of their marker genes ubiquitously, compared to previous Tg rats. We also evaluated immunological antigenicity against these marker proteins using conventional skin grafting, and discovered that the skin from lacZ-Tg rats was much less immunogenic than that of GFP-Tg. Nonetheless, GFP-positive cells from parental transgenic rats were available for the observation of cellular fate in an immune privilege site, such as the brain. We also examined the role of bone marrow-derived cells (BMDCs) in skin wound healing using the less immunogenic lacZ-Tg rat and autologous cell transplantation. Although transplantation of BMDCs enhanced wound healing at the injection site, BMDCs were not detected for a long times despite using a sensitive biological imaging system, suggesting the transient and limited contribution of autologous BMDC transplantation in wound healing. An animal model using our Tg-rat system may provide great benefits for the study of regenerative medicine, including cellular and tissue transplantation.

Materials and methods

Animals. An inbred rat strain, Lewis (LEW) (MHC haplotype: $RT1^l$), was purchased from Charles River Japan, (Yokohama, Japan). LacZ-expressing DA (CAG/LacZ-DA) transgenic rats (MHC haplotype: $RT1^a$) and GFP-expressing Wistar (CAG/GFP-Wistar) transgenic rats (MHC haplotype: $RT1^k$) have been described previously [4,5]. Both of the transgenes were driven under the CAG promoter [8]. All animals had free access to standard chow and drinking water, and were maintained on a 12-h light/dark cycle. All experiments in this study were performed in accordance with the Jichi Medical School Guide for Laboratory Animals.

Generation of transgenic rats. To generate ROSA/LacZ- and CAG/GFP-LEW Tg rats, the authentic microinjection technique was used as described previously [4]. Briefly, the *Nco*I and *Nhe*I fragment (LacZ cDNA) from a pMOD-LacZ plasmid (InvivoGen, San Diego, CA) was inserted into the *Nco*I and *Xba*I sites of a pBROAD2 expression plasmid (InvivoGen) containing ROSA26 promoter [9], and the *Pac*I fragment containing the promoter and coding sequence was injected into the fertilized Lewis rat egg. Transgene expression was examined by β-galactosidase staining (detailed below).

For the GFP-expression plasmid, GFP cDNA from a pEGFP vector (Clontech, Palo Alto, CA) was inserted into a pCAGGS expression plasmid [4,8], and the *Hin*dIII–*Sal*I fragment was injected into the fertilized Lewis rat egg. Transgene expression was confirmed under an excitation light (489 nm). In this study, hemizygous Tg rats (LEW-Tg(Rosa-LacZ)15Jmsk and LEW-Tg(CAG-GFP)ys) were used.

Detection of lacZ expression. Samples were embedded in OCT compound (Miles laboratory, IN), frozen in liquid nitrogen, and cut into thin (8–10 μm) sections under freezing conditions. Sections were fixed with a fixative solution (0.2% glutaraldehyde, 2 mM $MgCl_2$, and 5 mM EGTA) in phosphate-buffered saline (PBS) for 5 min at room temperature (RT), and washed three times in a washing solution (2 mM $MgCl_2$, 0.01% sodium deoxycholate, and 0.02% Nonidet-P40) in PBS. Specimens were treated with a β-gal staining solution (1 mg/ml of 5-bromo-4-chloro-3-indolyl-β-D-galactopyranoside, 2 mM $MgCl_2$, and 5 mM potassium hexacyanoferrate [III], 5 mM potassium hexacyanoferrate [II] trihydrate) at 37 °C for 1–4 h [10]. Eosin was then used for counter-staining.

To visualize lacZ expression in vivo and in vitro, an in vivo bioimaging system (IVIS) (Xenogen, Alameda, CA) was used. Animals were anesthetized using isoflurane (Abbot, Chicago, IL), and Beta-glo (Promega, Madison, WI) was administered locally to the artificial dermis or skin graft (50 μl of the reagent/animal). LacZ expression photo-images were taken by IVIS and quantified using Living Image software (Xenogen), which measured photon/s/cm^2/steradian. Longitudinal changes in lacZ expression of artificial dermis in the same animal were followed using IVIS.

Skin grafting. Skin transplantation was performed using 6- to 8-week-old female rats. Full-thickness donor skin grafts were transplanted onto a dorsal area of recipients under diethyl ether anesthesia using our coupled skin grafting method [11]. Grafted skins were fixed physically using 5–0 nylon tie-over sutures and bandages. Grafts were monitored regularly by visual and tactile inspection after the removal of the bandage on day 6, as described by Billingham and Medawar [12]. Rejection was defined as the start of contraction of the skin graft according to previously defined criteria [11].

Neurosphere preparation and transplantation into the injured brain. Neurospheres were prepared by culturing cells from the fetus of CAG/GFP-LEW Tg rats as described by Reynolds et al. [13]. GFP-positive fetuses of 14.5 day gestation were obtained from pregnant rats. After decapitation, brains were mechanically excised and collected in cold PBS. Each sample was mined with a razor blade following centrifugation for 500*g*, 10 min. The precipitate was resuspended in PBS containing 0.1% trypsin and 0.04% DNase, and then incubated at 37 °C for 30 min to facilitate dissociation into single cells. The dissociated cells were cultured in serum-free Dulbecco's modified Eagle's medium/Ham's F12 (DEMEM/F12: Gibco, Grand, Island, NY) with basic fibroblast growth factor (bFGF, 10 mg/ml, Sigma) and epidermal growth factor (EGF, 20 mg/ml, Sigma). GFP expression in the cultured cells was analyzed using a flow cytometer.

The left-middle cerebral artery (MCA) in adult male LEW rats was occluded for 60 min using the intraluminal filament method [14]. Five days after MCA occlusion, the rats were anesthetized with ketamine (60 mg/kg, ip) and xylazine (6 mg/kg, ip) and then placed in a stereotactic frame (Type SR-50 Narishige, Tokyo, Japan). GFP^+ neural stem cells (1.1×10^4 cells) were transplanted into the left side of the lateral ventricle through a glass micropipette.

After transplantation of the neurosphere, the host rats were sacrificed at 28 days. Each rat was perfused transcardially with heparinized saline followed by a phosphate-buffered solution containing 4% paraformaldehyde and 7.5% sucrose. The brains were removed and serially sectioned in the coronal plane at a thickness of 2-mm. GFP expression in each section was observed using a fluorescence stereoscopic microscope.

BMDC preparation and artificial dermis grafting. BMDCs were harvested by flushing femurs, tibiae and humeri of rats with ice cold PBS. Red blood cells were lysed with ACK buffer (150 mM NH_4Cl, 10 mM $KHCO_3$, and 0.1 mM EDTA, pH 7.2) at 4 °C for 30 min. Cells were then washed with PBS three times and re-suspended in PBS just before injection.

The head hair of rats was clipped under anesthetic conditions. Full-thickness skin defects (2-cm × 2-cm) were made on the head. The artificial dermis (Terudermis, Terumo, Tokyo, Japan) containing 10^7 BMDC cells (100 μl) was grafted onto the skin defects. As a control group, artificial dermis containing PBS (100 μl) was grafted. For histological evaluation, animals were killed 1, 2, 3, 4, and 8 weeks after transplantation, and specimens were stained using a β-gal solution.

Results

LacZ and GFP expression in inbred (Lewis) transgenic rats

In an effort to examine the expression pattern of newly developed transgenic rats, various organs were removed from transgenic animals and their expression pattern and intensity were determined. Regarding LacZ-LEW transgenic rats, we compared lacZ expression of the previously established LacZ-DA Tg (CAG/LacZ-DA) line [5] with that of the LacZ-LEW (ROSA/LacZ-LEW) line. While skeletal muscle and myocardium revealed strong lacZ expression in CAG/LacZ-DA rats, ROSA/LacZ-LEW rats showed weak and heterogeneous expression in these tissues (Fig. 1). In contrast, ROSA/LacZ-LEW rats showed superior expression in the liver (hepatocytes), skin (epidermis and hair follicles), small intestine, and cartilage, compared to CAG/LacZ-DA rats. Expression patterns of lacZ and intensity are summarized in Table 1. It is notable that bone marrow cells were not stained by this histological staining procedure, but their expression was visualized by the Beta-glo bioluminescent system (described later).

On the other hand, we also evaluated the GFP expression pattern between CAG/GFP-LEW and CAG/GFP-Wistar Tg rats. The new CAG/GFP-LEW line expressed GFP strongly and ubiquitously in most of the organs, compared with the former GFP-Tg line of Wistar [4] (Table 2). As shown in Fig. 2, representative organs such as the brain, liver, and intestine demonstrated higher levels of GFP-expression in the new GFP-LEW Tg line.

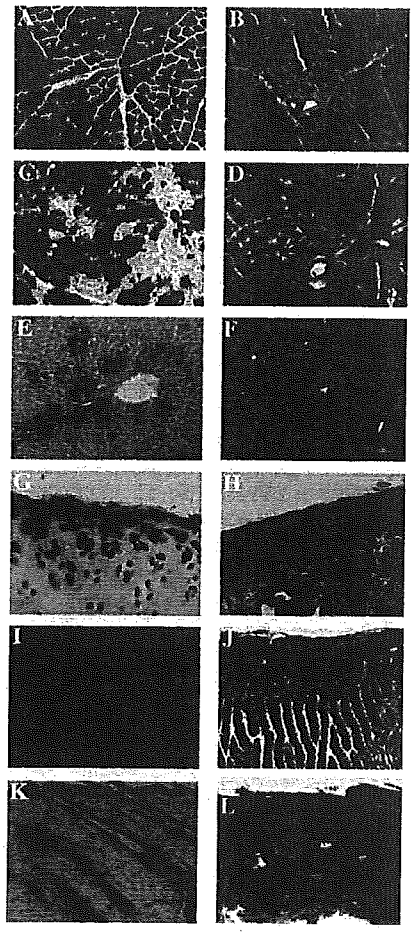

Fig. 1. Differential LacZ-expression pattern between CAG/LacZ-DA and ROSA/LacZ-LEW Tg rats. Tissues skeletal muscle (A,B), myocardium (C,D), liver (E,F), cartilage (G,H), small intestine (I,J), and skin (K,L) were removed from CAG/LacZ-DA (A,C,E,G,I, and K) [5] and ROSA/LacZ-LEW Tg rats (B,D,F,H,J, and L). Specimens were fixed with 0.2%-glutaraldehyde and stained with a β-gal staining solution (original magnification 100×). Experiments were performed two to three times, each with similar results.

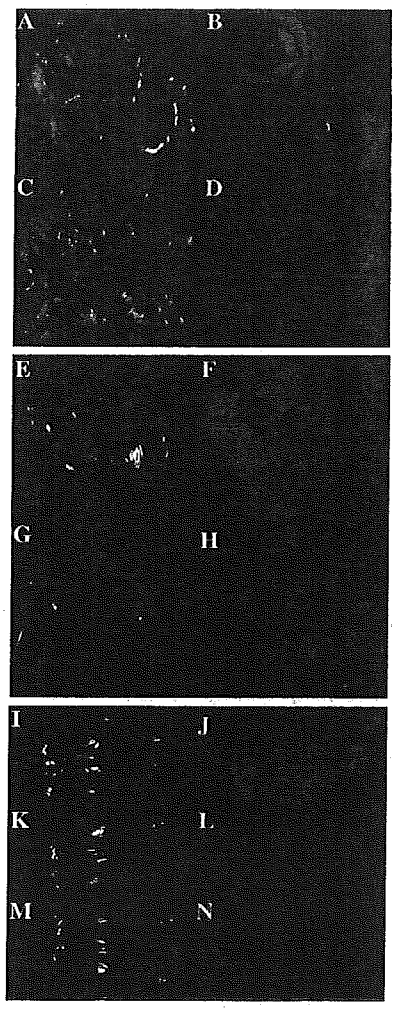

Fig. 2. Differential GFP-expression pattern between CAG/GFP-Wistar and CAG/GFP-LEW Tg rats. Representative organs (small intestine (A–D), liver (E–H), and brain (I–N)) were removed from CAG/GFP-LEW (A,B,E,F,I, and J) and CAG/GFP-Wistar Tg rats [4] (C,D,G,H,K, and L), and examined under a visible (A,C,E,G,I,K, and M) or 489 nm excitation light (B,D,F,H,J,L, and N). (M) and (N) represent wild-type LEW rats (as a negative control). Results derived from one of two independent experiments showing similar results.

Table 1
Differential expression profile between the adult CAG/LacZ-DA and ROSA/LacZ-LEW Tg rats

Organ	CAG/LacZ-DA	ROSA/LacZ-LEW
Brain	–	+
Heart	+++	+
Skeletal muscle	+++	+
Vessels	–	++
Liver	+	+++
Pancreas	++	++
Small intestine	+	+++
Kidney	+	+
Cartilage	++	+++
Nerve	–	–
Skin	++	+++
Bone[a]	–	–
Bone marrow	–	–

[a] Born matrix was LacZ-negative, but osteocytes were LacZ-positive.

Table 2
Differential expression profile of GFP between the adult CAG/GFP-Wistar and CAG/GFP-LEW Tg rats

Organ	CAG/GFP-Wister	CAG/GFP-LEW
Brain	+/–	+++
Eye	++	+++
Lung	+/–	+++
Heart	++	+++
Thymus	+	+++
Liver	+	+++
Pancreas	++	+++
Small intestine	+	+++
Colon	+	+++
Kidney	++	+++
Muscle	++	+++
Skin	+	+++

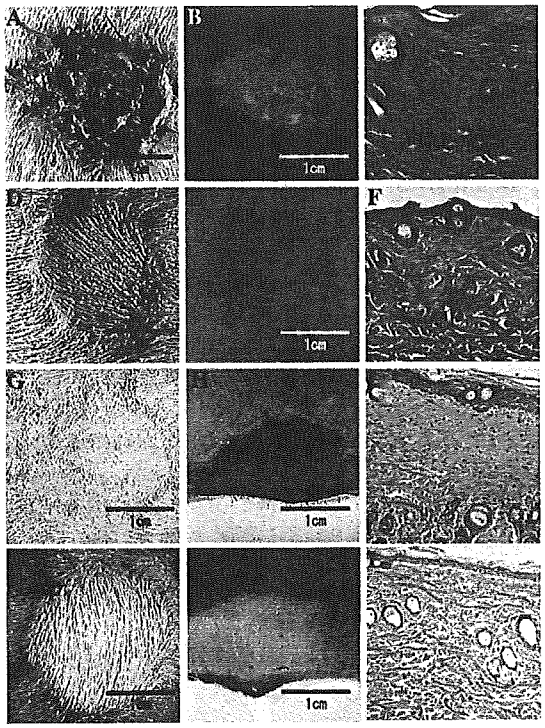

Fig. 3. Skin transplantation between transgenic and wild-type rats. (A–F) represent typical skin grafts between CAG/GFP-LEW and wild-type LEW rats at 14 days after transplantation. The skin graft from CAG/GFP-LEW on wild-type LEW rats under a visible (A) or 489 nm excitation light (B). Note hyperkeratosis and erythema with many cellular infiltrates (C) in the skin graft. The skin graft of wild-type LEW on CAG/GFP-LEW rats under a visible (D) or 489 nm excitation light (E). (F) Microscopic appearance indicates hair follicles without cell infiltrates at 24 days post-transplantation (hematoxylin and eosin (H and E), 200× magnification). (G) The skin graft of ROSA/LacZ-LEW vs. wild-type rats at 28 days post-transplantation. (H) Blue area represents the skin border resulting from β-gal staining. Note the almost histologically intact skin, except for premature hair growth with fewer cell infiltrations (H and E, 200× magnification). The skin graft from wild-type LEW rats placed onto ROSA/LacZ-LEW Tg rats has an appearance equivalent to the skin graft from the wild-type placed onto CAG/GFP-LEW rats at 28 days post-transplantation (J,K, β-gal stain; L,H, and E, 200× magnification).

LacZ is less immunogenic than GFP

The transplantation of cells and tissues is a well-established strategy used in an effort to evaluate the nature of cellular processes. Transplanted cells expressing a marker protein, however, have occasionally disappeared during the observation period, even with syngeneic transplantation, and this has sometimes been explained in terms of immunogenicity [15–17]. Therefore, we evaluated how tissues from newly developed inbred Tg animals possess immunogenic potential. The skin grafting model was used to clarify the antigenic relationship between Tg and wild-type LEW rats because the skin is the most immunogenic organ and the grafting technique provides an easy experimental procedure. The skin grafts of either CAG/GFP-LEW or ROSA/LacZ-LEW rats were transplanted onto a dorsal area of parental LEW rats. The skin of CAG/GFP-LEW Tg rats resulted in graft rejection (Figs. 3A–C); this rejection reaction occurred within 6–9 days after skin transplantation (Table 3), suggesting acute graft rejection. By contrast, Rosa/LacZ-LEW skin graft remained intact for more than 90 days (Figs. 3G–I). Microscopic studies showed that CAG/GFP-LEW Tg skin grafting introduced more intense cellular infiltrate than ROSA/LacZ skin grafting (Figs. 3C and I). These cellular infiltrates represented $CD8^+$ T cells, while $CD4^+$ T cells were scarcely observed using immunostaining (data not shown). Rejection patterns after grafting are summarized in Table 3. Skin grafting of wild-type rats to both Tg animals did not show any rejection reaction more than 30 days after transplantation (Figs. 3D–F, and J–L). These results therefore demonstrate that LacZ is less immunogenic than GFP, and suggest that cells from ROSA/LacZ-LEW Tg rats may be more useful for the evaluation of cellular process through a transplantation technique than those of GFP-LEW Tg rats.

Table 3
Skin graft survival in Lewis rats

Donor	Recipient	*n*	Graft survival (days)	MST	Median (days)
GFP-Tg	WT	6	6, 6, 6, 6, 6, 9	6.5	6
WT	GFP-Tg	5	>60, >60, >60, >60, >60	>60	>60
LacZ-Tg	WT	2	>90, >90	>90	>90
WT	LacZ-Tg	2	>90, >90	>90	>90

WT, wild-type; MST, mean survival time.

Immune privilege site accepts GFP-Tg-derived neural progenitor cells

Notwithstanding the immunogenic response of GFP, the use of cells from GFP-Tg is still attractive for studies of cellular monitoring due to the stable marker expression and easy visualization under excitation light. Since the brain is well known as an immunologically privileged site, we further examined the cellular fate of neural progenitor cells from CAG/GFP-LEW Tg rats without any immunosuppressive drugs in a rat cerebral infarction model. Neural progenitor cells were established from E14.5 of CAG/GFP-LEW Tg rats and maintained in vitro for 20 days under appropriate culture conditions (see Materials and methods). Neurosphere cells strongly expressed GFP (Fig. 4A) and nestin (Fig. 4B), and kept the phenotype as the neural progenitor. The sphere cells were then transplanted stereotactically into the cerebral ventricle space of wild-type LEW rats at 5 days post-infarction. As shown in Fig. 4D, GFP-positive cells accumulated in the cerebral infarction area and were able to survive. Thus, even if GFP is highly immunogenic, GFP-positive cells are still useful and attractive materials for the study of cellular fate in immune privilege sites.

Contribution of ROSA/LacZ-LEW Tg-derived BMDCs to skin wound healing

BMDCs are also utilized in a transplantation strategy to restore and form damaged tissues. Considering the less immunogenic lacZ and sensitive luminescence assay for the expression of lacZ, we evaluated the contribution of BMDCs to skin wound healing. LacZ-expression of BMDCs was visualized in the presence of a luminescent substrate (Beta-glo, Promega), and at least 2000 cells were able to give rise to successful imaging in vitro (5×10^6 photons) (Fig. 5A). Full-thickness skin defects (2-cm × 2-cm) were made on the head of wild-type LEW rats, and BMDCs (10^7 cells/100 μl) from ROSA/LacZ-LEW rats with the artificial dermis (Terudermis) were transplanted into the skin defects of these rats (artificial dermis plus PBS 100 μl was grafted as the experimental control). Substantial luminescent images were only obtained for a few days (Figs. 5B and C), but BMDCs contributed to skin wound healing, as also

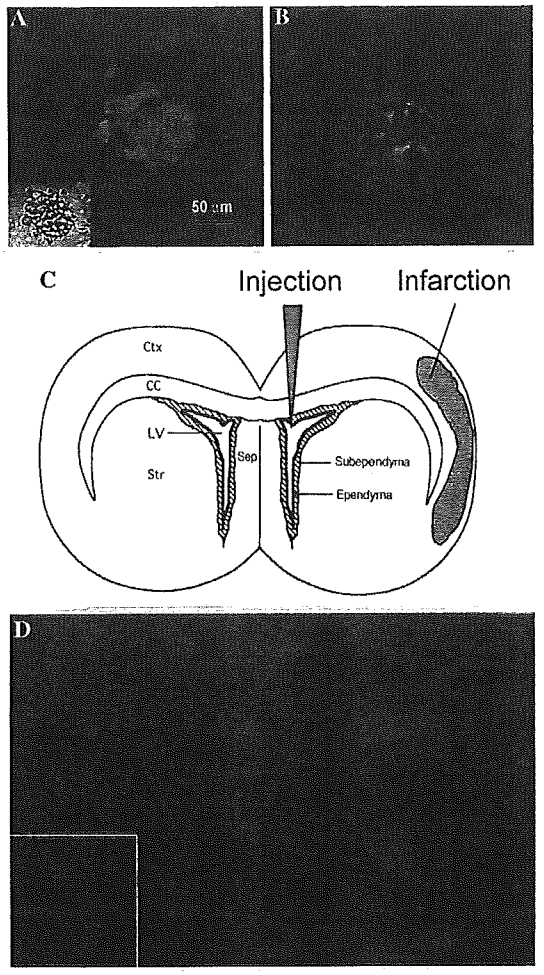

Fig. 4. Migration of neural progenitor-derived cells to the cerebral infarction area. (A) Neural progenitor cells from CAG/GFP-LEW Tg rats express substantial levels of GFP under a 489 nm excitation light 40× magnification). (B) Nestin (red color) was expressed in neural progenitor cells from CAG/GFP-LEW Tg rats (40× magnification). Cells were stained with anti-Nestin mAb (clone# Rat401) (Chemicon International, Temecula, CA) and followed by anti-mouse IgG-Cy3 (Chemicon International). Green color represents GFP. (C) Representative scheme of stereotactic microinjection to the cerebral ventricle. A glass micropipette was placed at an anterior position of 0.0-mm and lateral position of +1.5-mm from the center of the bregma, and cannula depth was 3.3-mm below the surface of the dura matter. The cell suspension (10 μl) was infused over 10 min. Gray area represents the infarction. (D) Accumulation of GFP^+ neural progenitor-derived cells to the cerebral infarction area. Neural progenitor cells (1.1×10^4 cells) from CAG/GFP-LEW Tg rats were injected into the cerebral ventricle, and transverse sections were made at 28 days post-cell transplantation (under a 489 nm excitation light, 10× magnification). One of two independent experiments with similar results.

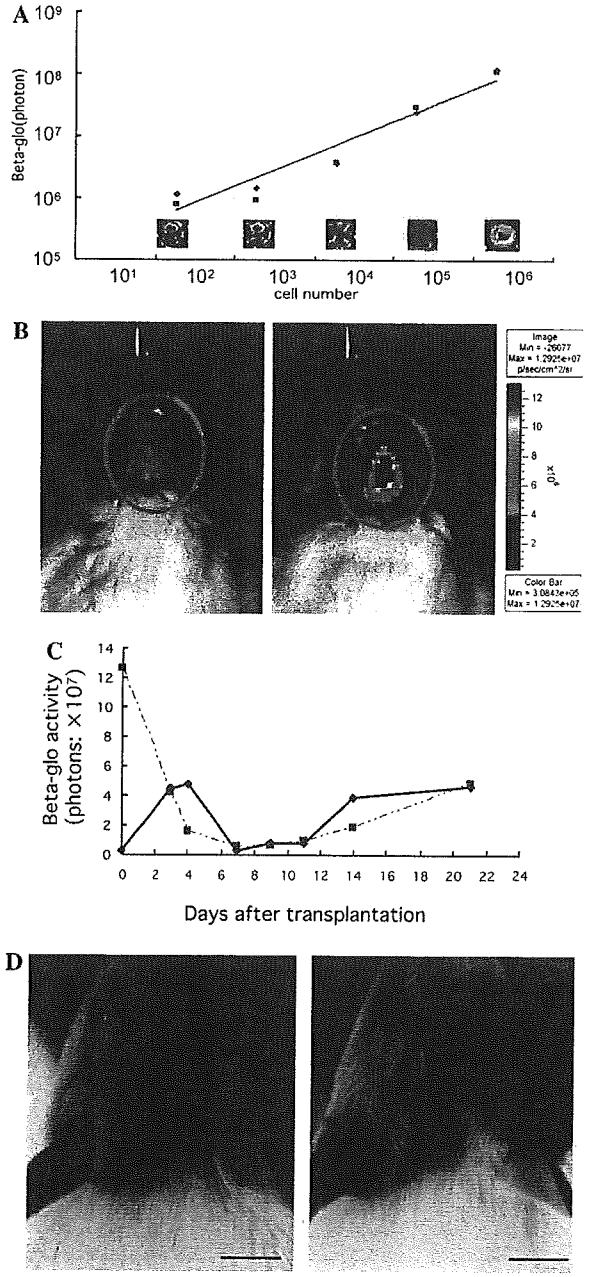

Fig. 5. Effect of BMDCs on skin wound healing. (A) Visualization of LacZ-expressing BMDCs. The number of BMDC cells from the ROSA/LacZ-LEW Tg rat was analyzed by an in vivo bio-imaging system using Beta-glo (Promega). At least 2000 cells contributed to the substantial imaging obtained from the in vitro investigation ($\sim 5 \times 10^6$ photons). Photons were correlated with cell number ($y = 1.3 \times 10^5\, x^r$, $r = 0.53$). (B) In vivo imaging of BMDCs from the ROSA/LacZ-LEW Tg rat at 2 days post-transplantation. Full-thickness skin defects (20-mm × 20-mm) were made on the head of rats, and BMDCs (10^7 cells) from ROSA/LacZ-LEW Tg rats with the artificial dermis (Terudermis) were transplanted onto the skin defects (right). The left panel represents a mock treatment. (C) Time-course quantification of LacZ-expressing BMDCs. The BMDC-treated animals were analyzed by the in vivo bio-imaging system every other day. (D) Representative image of wound healing using BMDCs at 21 days after post-operation. It is notable that the wound area decreased following administration of BMDCs (right panel), compared with that of the mock treatment (left panel). One of two independent experiments with similar results.

recently demonstrated by Yamaguchi et al. [18] (Fig. 5D). The wound area reduction rate was 9.6 ± 2.7% in the BMDC-administered group and 12.9 ± 6.9% in the control group. Nonetheless, their cellular signals were equivalent to the background level after 4 days post-grafting, and cell fate was not monitored throughout the healing period (Fig. 5C). These results therefore suggest that BMDCs can indeed enhance skin wound healing, but their contribution may be low and perhaps transitory.

Discussion

In this study, we established new inbred transgenic LEW rats with LacZ and GFP markers. Three remarkable features were demonstrated in our examinations: (1) ROSA/LacZ-Tg was strongly expressed in the liver, small intestine, cartilage and skin, and expressed to a lesser degree in the heart and skeletal muscle, in comparison with the former established CAG/LacZ-DA Tg line; (2) CAG/GFP-LEW Tg expressed GFP ubiquitously and strongly in all of the tissues we examined; and (3) cells from ROSA/LacZ-Tg were less immunogenic than those of CAG/GFP-Tg. We also demonstrated potential applications for cells from these transgenic animals by means of the cell transplantation technique.

It has been established that a generation of transgenic animals using an appropriate marker gene provides a useful strategy to monitor cellular fate, including migration, proliferation, and differentiation [9,19,20]. These cellular events play significant roles in organ development and tissue regeneration. To this purpose, our research groups and those of others have tried to generate LacZ and GFP transgenic rats. Previous established lines of LacZ-expressing Tg rats did not achieve ubiquitous lacZ expression, and only limited tissues such as the heart and skeletal muscle expressed enough of the marker gene, even though it had been driven under the ubiquitous promoter (CAG promoter) [5]. In this study, we hired the ROSA26 promoter [9] to obtain ubiquitous gene expression. In contrast to our previous line using the CAG promoter [5], lacZ expression was broadened to other tissues, whereas heart and skeletal muscle were less expressive, and it may be argued that such differential gene expression depended on the genomic integration sites of the expression plasmid. Furthermore, the new CAG/GFP-LEW Tg line also gave rise to much stronger GFP expression in more tissues. Indeed, the mouse versions of these marker genes have been used elsewhere [19,20], but their further use for biomedical research such as tissue or organ transplantation may be restricted due to limitations imposed by body size. Rats have provided fabulous animal models for neurological research investigations [21,22]. Thus, the use of these

Tg-rats allows for the potential elucidation of the uncharacterized regeneration process.

GFP is a fluorescent product of the jellyfish (*Aequorea victria*) and is used for a variety of biological experiments as a reporter molecule [19]. While GFP possesses advantages for the non-invasive imaging of viable cells, GFP-positive cells are still considered potential xeno-antigens [15,16]. Our authentic skin grafting experiments showed that GFP induced striking immune responses, but lacZ was less immunogenic than GFP (Fig. 3 and Table 3). Thus, long-term studies of GFP^+ cell transplantation should be limited to immune privilege sites (e.g., brain and testis), and it is much safer to use LacZ-positive cells in other sites.

Furthermore, although it was pointed out that constitutive expression of GFP might affect cellular differentiation and proliferation in human cells [23], our preliminary experiments using neurosphere cells from CAG/GFP-LEW Tg rats did not show that fluorescent intensity (amount of GFP) induced any change in their differentiation status, compared with that of wild-type rats (data not shown). We therefore consider that GFP-positive cells of rats are still a useful tool for the study of neural development and regeneration.

We presented a few experimental applications using newly developed Tg rats. Stereotactic injection of GFP-positive neural progenitors showed migration and accumulation from the safe cerebral ventricle to the infarction area. It has recently been reported that this biological event is strongly associated with the chemokine receptor CXCR4 and the ligand CXCL12/SDF-1 [24,25]. Rat neural progenitors from our transgenic line expressed significant levels of CXCR4 and the cerebral infarction area revealed enhanced mRNA expression of CXCL12 (data not shown). We therefore speculated that those cells were activated and targeted by the interaction of CXCR4 with CXCL12. Furthermore, since there are emerging data suggesting that the axis of CXCR4 and CXCL12 enhances survival of various cells [26,27], it is likely that cell survival, as well as chemotactic migration, may contribute to the accumulation of GFP-positive neural progenitor-derived cells in the infarction area.

As with the case shown by Yamaguchi et al. [18], BMDCs administered to a wound area shortened the healing period. Indeed, a limited number of BMDCs eventually differentiated into myofibroblasts, but their proliferation at wound sites was less frequently observed. Thus, the contribution of administered BMDCs to wound healing may involve an appropriate supply of certain kinds of beneficial growth factors. Although similar results have been reported by others [28–30], our in vivo bio-imaging studies of live animals substantially support the above speculations by providing precise data on the fate of BMDCs at wound healing sites.

Since the rat is larger than the mouse, studies using the former animal make available various physiological techniques that may prove to have biological significance. A variety of rat experimental systems, including disease models, have been developed for over a century. Coupled with recent advances in genetic engineering of the rat, the transgenic rats presented in this report should provide innovative animal tools and help to broaden understanding in new biomedical research fields, such as regeneration medicine.

Acknowledgments

We thank Dr. Masatsugu Udeda (YS New Technology Institute, Tochigi, Japan) for kindly providing GFP transgenic Lewis rats, Dr. Jun-ichi Miyazaki (Osaka University, Graduate School of Medicine, Osaka, Japan) for providing the pCAGGS plasmid, and Dr. Kuniko Shimazaki (Department of Physiology, Jichi Medical School, Tochigi, Japan) for kindly supporting the cerebral stereotactic injection study. We thank Ms. Yasuko Sakuma, Ms. Megumi Hata, and Ms. Harumi Kawana for their skillful technical assistance. This study was supported by grants to E.K. from the Drug Innovation Program of the Japan Health Science Foundation, MEXT, HITE-KU (2003), and COE Program (2003). The transgenic rat embryo is available from the Health Science Research Resources Bank at hsrrb@osa.jhsf.or.jp.

References

[1] D. Orlic, J. Kajstura, S. Chimenti, I. Jakoniuk, S.M. Anderson, B. Li, J. Pickel, R. McKay, B. Nadal-Ginard, D.M. Bodine, A. Leri, P. Anversa, Bone marrow cells regenerate infarcted myocardium, Nature 410 (2001) 701–705.

[2] S. Pluchino, A. Quattrini, E. Brambilla, A. Gritti, G. Salani, G. Dina, R. Galli, U. Del Carro, S. Amadio, A. Bergami, R. Furlan, G. Comi, A.L. Vescovi, G. Martino, Injection of adult neurospheres induces recovery in a chronic model of multiple sclerosis, Nature 422 (2003) 688–694.

[3] R. Galli, A. Gritti, L. Bonfanti, A.L. Vescovi, Neural stem cells: An overview, Circ. Res. 92 (2003) 598–608.

[4] Y. Hakamata, K. Tahara, H. Uchida, Y. Sakuma, M. Nakamura, A. Kume, T. Murakami, M. Takahashi, R. Takahashi, M. Hirabayashi, M. Ueda, I. Miyoshi, N. Kasai, E. Kobayashi, Green fluorescent protein-transgenic rat: A tool for organ transplantation research, Biochem. Biophys. Res. Commun. 286 (2001) 779–785.

[5] M. Takahashi, Y. Hakamata, T. Murakami, S. Takeda, T. Kaneko, K. Takeuchi, R. Takahashi, M. Ueda, E. Kobayashi, Establishment of lacZ-transgenic rats: A tool for regenerative research in myocardium, Biochem. Biophys. Res. Commun. 305 (2003) 904–908.

[6] Y. Sato, Y. Igarashi, Y. Hakamata, T. Murakami, T. Kaneko, M. Takahashi, N. Seo, E. Kobayashi, Establishment of Alb-DsRed2 transgenic rat for liver regeneration research, Biochem. Biophys. Res. Commun. 311 (2003) 478–481.

[7] Y. Sato, H. Endo, T. Ajiki, Y. Hakamata, T. Okada, T. Murakami, E. Kobayashi, Establishment of Cre/LoxP recombination system in transgenic rats, Biochem. Biophys. Res. Commun. 319 (2004) 1197–1202.
[8] H. Niwa, K. Yamamura, J. Miyazaki, Efficient selection for high-expression transfectants with a novel eukaryotic vector, Gene 108 (1991) 193–199.
[9] B.P. Zambrowicz, A. Imamoto, S. Fiering, L.A. Herzenberg, W.G. Kerr, P. Soriano, Disruption of overlapping transcripts in the ROSA β geo 26 gene trap strain leads to widespread expression of β-galactosidase in mouse embryos and hematopoietic cells, Proc. Natl. Acad. Sci. U S A 94 (1997) 3789–3794.
[10] M. Takahashi, Y. Hakamata, K. Takeuchi, E. Kobayashi, Effects of different fixatives on β-galactosidase activity, J. Histochem. Cytochem. 51 (2003) 553–554.
[11] E. Kobayashi, K. Kawai, Y. Ikarashi, M. Fujiwara, Mechanism of the rejection of major histocompatibility complex class I-disparate murine skin grafts: rejection can be mediated by $CD4^+$ cells activated by allo-class I + II antigen in $CD8^+$ cell-depleted hosts, J. Exp. Med. 176 (1992) 617–621.
[12] R.E. Billingham, P.B. Medawar, The technique of free skin grafting in mammals, J. Exp. Biol. 28 (1951) 385–405.
[13] B.A. Reynolds, W. Tetzlaff, S. Weiss, A multipotent EGF-responsive striatal embryonic progenitor cell produces neurons and astrocytes, J. Neurosci. 12 (1992) 4565–4574.
[14] E.Z. Longa, P.R. Weinstein, S. Carlson, R. Cummins, Reversible middle cerebral artery occlusion without craniectomy in rats, Stroke 20 (1989) 84–91.
[15] R. Stripecke, M. Carmen Villacres, D. Skelton, N. Satake, S. Halene, D. Kohn, Immune response to green fluorescent protein: Implications for gene therapy, Gene Ther. 6 (1999) 1305–1312.
[16] J.O. Brubaker, C.M. Thompson, L.A. Morrison, D.M. Knipe, G.R. Siber, R.W. Finberg, Th1-associated immune responses to β-galactosidase expressed by a replication-defective herpes simplex virus, J. Immunol. 157 (1996) 1598–1604.
[17] A. Izembart, E. Aguado, O. Gauthier, D. Aubert, P. Moullier, N. Ferry, In vivo retrovirus-mediated gene transfer to the liver of dogs results in transient expression and induction of a cytotoxic immune response, Hum. Gene Ther. 10 (1999) 2917–2925.
[18] Y. Yamaguchi, T. Kubo, T. Murakami, M. Takahashi, Y. Hakamata, E. Kobayashi, S. Yoshida, K. Hosokawa, K. Yoshikawa, S. Itami, Bone marrow cells differentiate into wound myofibroblasts and accelerate the healing of wounds with exposed bones when combined with an occlusive dressing, Br. J. Dermatol. (in press).
[19] M. Chalfie, Y. Tu, G. Euskirchen, W.W. Ward, D.C. Prasher, Green fluorescent protein as a marker for gene expression, Science 263 (1994) 802–805.
[20] M. Okabe, M. Ikawa, K. Kominami, T. Nakanishi, Y. Nishimune, Green mice as a source of ubiquitous green cells, FEBS Lett. 407 (1997) 313–319.
[21] O. Szentirmai, B.S. Carter, Genetic and cellular therapies for cerebral infarction, Neurosurgery 55 (2004) 283–286, discussion 296–297.
[22] M. Murray, D. Kim, Y. Liu, C. Tobias, A. Tessler, I. Fischer, Transplantation of genetically modified cells contributes to repair and recovery from spinal injury, Brain Res. Brain Res. Rev. 40 (2002) 292–300.
[23] A. Martinez-Serrano, A. Villa, B. Navarro, F.J. Rubio, C. Bueno, Human neural progenitor cells: Better blue than green? Nat. Med. 6 (2000) 483–484.
[24] D.J. Ceradini, A.R. Kulkarni, M.J. Callaghan, O.M. Tepper, N. Bastidas, M.E. Kleinman, J.M. Capla, R.D. Galiano, J.P. Levine, G.C. Gurtner, Progenitor cell trafficking is regulated by hypoxic gradients through HIF-1 induction of SDF-1, Nat. Med. 10 (2004) 858–864.
[25] J. Yamaguchi, K.F. Kusano, O. Masuo, A. Kawamoto, M. Silver, S. Murasawa, M. Bosch-Marce, H. Masuda, D.W. Losordo, J.M. Isner, T. Asahara, Stromal cell-derived factor-1 effects on ex vivo expanded endothelial progenitor cell recruitment for ischemic neovascularization, Circulation 107 (2003) 1322–1328.
[26] H.E. Broxmeyer, S. Cooper, L. Kohli, G. Hangoc, Y. Lee, C. Mantel, D.W. Clapp, C.H. Kim, Transgenic expression of stromal cell-derived factor-1/CXC chemokine ligand 12 enhances myeloid progenitor cell survival/antiapoptosis in vitro in response to growth factor withdrawal and enhances myelopoiesis in vivo, J. Immunol. 170 (2003) 421–429.
[27] T. Murakami, A.R. Cardones, S.T. Hwang, Chemokine receptors and melanoma metastasis, J. Dermatol. Sci. 36 (2004) 71–78.
[28] E.V. Badiavas, M. Abedi, J. Butmarc, V. Falanga, P. Quesenberry, Participation of bone marrow-derived cells in cutaneous wound healing, J. Cell. Physiol. 196 (2003) 245–250.
[29] E.V. Badiavas, V. Falanga, Treatment of chronic wounds with bone marrow-derived cells, Arch. Dermatol. 139 (2003) 510–516.
[30] Y. Yamaguchi, S. Yoshida, Y. Sumikawa, T. Kubo, K. Hosokawa, K. Ozawa, V.J. Hearing, K. Yoshikawa, S. Itami, Rapid healing of intractable diabetic foot ulcers with exposed bones following a novel therapy of exposing bone marrow cells and then grafting epidermal sheets, Br. J. Dermatol. 151 (2004) 1019–1028.

TEF, an antiapoptotic bZIP transcription factor related to the oncogenic E2A-HLF chimera, inhibits cell growth by down-regulating expression of the common β chain of cytokine receptors

Takeshi Inukai, Toshiya Inaba, Jinjun Dang, Ryoko Kuribara, Keiya Ozawa, Atsushi Miyajima, Wenshu Wu, A. Thomas Look, Yojiro Arinobu, Hiromi Iwasaki, Koichi Akashi, Keiko Kagami, Kumiko Goi, Kanji Sugita, and Shinpei Nakazawa

Gain and/or loss of function mediated by chimeric transcription factors generated by nonrandom translocations in leukemia is a key to understanding oncogenesis. E2A–hepatic leukemia factor (HLF), a chimeric basic region/leucine zipper (bZIP) transcription factor expressed in t(17;19)–positive leukemia cells, contributes to leukemogenesis through its potential to inhibit apoptosis. To identify physiologic counterparts of this chimera, we investigated the function of other bZIP factors that bind to the same DNA sequence recognized by E2A-HLF. Here, we show that thyrotroph embryonic factor (TEF), which shares a high level of sequence identity with HLF and recognizes the same DNA sequence, is expressed in a small fraction of each subset of hematolymphoid progenitors. When TEF was introduced into FL5.12 interleukin 3 (IL-3)–dependent cells, TEF protected the cells from apoptosis due to IL-3 deprivation. Unexpectedly, TEF also almost completely down-regulated expression of the common β (βc) chain of cytokine receptors. Consequently, TEF-expressing cells accumulated in G_0/G_1 phase without undergoing apoptosis. These findings suggest that TEF is one of the apoptotic regulators in hematopoietic progenitors and controls hematopoietic-cell proliferation by regulating the expression of the βc chain. In contrast, E2A-HLF promoted cell survival more efficiently than TEF but did not down-regulate βc chain expression, suggesting that E2A-HLF retains ideal properties for driving leukemic transformation. (Blood. 2005;105:4437-4444)

Introduction

Since key systems that regulate cell survival have been conserved through evolution, relatively simple organisms such as *Caenorhabditis elegans* often provide insight into the complex mechanisms that control cell fate in mammals.[1] The genetic approach demonstrated that 2 factors, cell death specification protein 1 (CES-1) and CES-2, regulate the programmed cell death of serotonergic neurosecretory motor (NSM) neurons in *C elegans* in a cell type–specific fashion.[2] Further studies revealed that CES-2 is a transcription factor that belongs to the basic region/leucine zipper (bZIP) superfamily (Figure 1).[3] CES-2 negatively regulates CES-1, a member of the snail family of zinc finger transcription factors,[4] and CES-1 appears to determine the fate of NSM sisters by negatively regulating the expression of *egl1*, a BH3-only proapoptotic member of the B cell lymphoma (Bcl-2) superfamily.[5-7]

Transcription factors that bind to the DNA sequence elements recognized by CES-2 might play important roles in cell type–specific cell death in mammals. The E2A–hepatic leukemia factor (HLF) fusion transcription factor is a good example. This chimera is derived from childhood acute pro-B-cell leukemia harboring a t(17;19) chromosomal translocation.[8-10] It contains the transactivation domains of E2A and the bZIP DNA-binding and dimerization domain of HLF (Figure 1). E2A-HLF promotes the anchorage-independent growth of murine fibroblasts as a homodimer that depends on both the transactivation domain of E2A and the bZIP domain of HLF.[11,12] E2A-HLF induces the expression of annexin II,[13] annexin V, and sushi-repeat protein upregulated in leukemia (SRPUL),[14] which have been postulated to play paraneoplastic roles in coagulopathies and bone invasion, as well as groucho-related genes, and E2A-HLF also suppresses Runt-related 1 (RUNX1).[15] In addition, we and others established transgenic mice expressing *E2AHLF* that develop T-lineage lymphoid malignancies.[16,17] Of note, we demonstrated that E2A-HLF binds avidly to the sequence recognized by CES-2 and protects cells from apoptosis due to growth factor deprivation without promoting cell proliferation.[18-20] The close homology between the bZIP domains of HLF and CES-2 suggests that E2A-HLF subverts a cell-death pathway through a mechanism similar to that used by CES-2 in the worm. Indeed, we have identified SLUG, a zinc finger transcription factor closely related to CES-1, as one of the downstream targets of E2A-HLF in human leukemias associated with the 17;19 translocation and found that SLUG has antiapoptotic potential.[21,22]

These findings suggest that a cell-death pathway in mammalian hematopoietic cells is normally regulated by bZIP factors that exhibit a DNA-binding specificity similar to that of CES-2 or E2A-HLF. HLF is obviously a good candidate for the regulator of apoptosis in hematopoiesis; however, HLF is not expressed in

From the Department of Pediatrics, School of Medicine, University of Yamanashi, Yamanashi, Japan; Department of Molecular Oncology, Research Institute for Radiation Biology and Medicine, Hiroshima University, Hiroshima, Japan; Department of Experimental Oncology, St Jude Children's Research Hospital, Memphis, TN; Division of Hematology, Jichi Medical School, Tochigi, Japan; Institute of Molecular and Cellular Bioscience, the University of Tokyo, Tokyo, Japan; Pediatric Oncology Department and Department of Cancer Immunology & AIDS, Dana-Farber Cancer Institute, Boston, MA.

Submitted August 2, 2004; accepted January 2, 2005. Prepublished online as *Blood* First Edition Paper, January 21, 2005; DOI 10.1182/blood-2004-08-2976.

Reprints: Takeshi Inukai, Department of Pediatrics, School of Medicine, University of Yamanashi, 1110 Shimokato, Tamaho-cho, Nakakoma-gun, Yamanashi 409-3898, Japan. e-mail: tinukai@yamanashi.ac.jp

The publication costs of this article were defrayed in part by page charge payment. Therefore, and solely to indicate this fact, this article is hereby marked "advertisement" in accordance with 18 U.S.C. section 1734.